

Spatio-temporal variability of concentrations and speciation of particulate matter across Spain in the CALIOPE modeling system

M.T. Pay^a, P. Jiménez-Guerrero^b, O. Jorba^a, S. Basart^a, X. Querol^c, M. Pandolfi^c, J.M. Baldasano^{a,d,*}

^aEarth Sciences Department, Barcelona Supercomputing Center-Centro Nacional de Supercomputación, Barcelona, Spain

^bPhysics of the Earth, University of Murcia, Spain

^cInstitute of Environmental Assessment and Water Research, Spanish Research Council (IDAEA-CISC), Barcelona, Spain

^dEnvironmental Modeling Laboratory, Technical University of Catalonia, Barcelona, Spain

ARTICLE INFO

Article history:

Received 14 June 2011

Received in revised form

16 August 2011

Accepted 22 September 2011

Keywords:

Aerosols

Desert dust

Air quality

Emissions

Geochemistry

ABSTRACT

The CALIOPE high-resolution air quality modeling system (4 km × 4 km, 1 h) estimates particulate matter from two aerosol models, CMAQv4.5 (AERO4) and BSC-DREAM8b. While CMAQv4.5 calculates biogenic, anthropogenic and sea-salt aerosols; BSC-DREAM8b provides hourly estimates of the natural mineral dust contribution from North Africa deserts. This paper presents an evaluation of the CALIOPE system to reproduce the spatial and temporal variability levels of PM_{2.5}, PM₁₀ and chemical composition (nitrate, non-marine sulfate, ammonium, organic and elemental carbon, sea-salt, and desert dust) across Spain. The evaluation is performed against ground-based observations for the year 2004, when a number of time series of chemically speciated compounds were available. A new data set of Saharan dust PM₁₀ concentration is used to evaluate the PM₁₀ contribution modeled by BSC-DREAM8b. The results indicate that both natural aerosol sea-salt and desert dust accomplish the model performance criteria (MFE ≤ 75% and MFB ± 60%). Modeled PM₁₀ sea-salt is highly dependent on wind speed and presents high correlation with experimental data in coastal areas ($r = 0.67$). The BSC-DREAM8b is able to reproduce the daily variability of the observed levels of desert dust and most of the outbreaks affecting southern Spain. Species in the equilibrium (e.g. sulfate/nitrate/ammonium) are highly correlated each other and show high dependency on ammonia emissions. Non-marine sulfate and ammonium are underestimated by a factor of 3. An underestimation of nitrate was also seen (factor of 2). Fine carbonaceous aerosols present the highest underestimations (factor of 4) in part related to the state-of-the-science concerning secondary organic aerosol formation pathways. Spatial and seasonal variability of PM_{2.5}, PM₁₀ and their chemical compounds increase the correlation with observations when multiplicative bias-correction factors for the aforementioned underestimated species are taken into account. Furthermore, simulated spatial and seasonal patterns of aerosol agree with those described in related studies based on experimental values.

© 2011 Elsevier Ltd. All rights reserved.

1. Introduction

Particulate matter (PM) is of major scientific interest due to its demonstrated impact on human health (WHO, 2006), ecosystems (Lovett et al., 2000), Earth's climate (Jacobson, 2001; Ramanathan et al., 2001; IPCC, 2007) and visibility (Hyslop and White, 2008). Although air quality in Europe has improved substantially over the past decades, air pollution by PM is a major threat to human health (EEA, 2010). Not only do concentrations determine the effects of particles on human health, but also (1) their size, conditioning the

degree of penetration into the respiratory system, (2) their composition, since the toxicity of the particles depends on the occurrence of specific hazardous PM compounds (Brauer et al., 1995) and (3) time of exposure. Although the effects of long-term exposure are much more uncertain than the effects of short-term exposure, they are believed to have a greater effect on health (Dockery et al., 1993; Pope et al., 2002). Recent studies carried out in Spain demonstrate that the levels of the finest PM fractions are important risk factors for daily cardiovascular mortality (Pérez et al., 2009; Maté et al., 2010) increasing the number of hospital admissions due to pollution caused by fine-particles (Linares and Díaz, 2010a,b). Current European standards on air quality, driven by the directive 2008/50/EC (European Commission, 2008), set an annual limit value for PM₁₀ (particles below 10 μm in diameter) of 40 μg m⁻³; and a daily mean value of 50 μg m⁻³ should not be exceeded 35 times per year. For the

* Corresponding author. Earth Science Department, Barcelona Supercomputing Center-Centro Nacional de Supercomputación (BSC-CNS), Jordi Girona 29, Edificio Nexus II, 08034 Barcelona, Spain. Tel.: +34 93 413 77 19; fax: +34 93 413 77 21.

E-mail address: jose.baldasano@bsc.es (J.M. Baldasano).

first time, a European directive introduces a limit value for PM_{2.5} (particles below 2.5 μm in diameter) in the air quality standards to be accomplished in two stages: Stage I, a mean maximum annual limit value of 25 $\mu\text{g m}^{-3}$ (deadline: 2015); and Stage II, a mean maximum annual limit value of 20 $\mu\text{g m}^{-3}$ (deadline: 2020).

A number of studies (e.g. Sanz et al., 2000; Dueñas et al., 2002; Millán et al., 2002; Querol et al., 2004, 2008; Ribas and Peñuelas, 2004; Escudero et al., 2007a) show that the Iberian Peninsula (IP) exceeds some of the thresholds of air quality established in the legislation. Exceedances of the PM₁₀ limit values were not only caused by anthropogenic emissions but also the long-range transport of atmospheric mineral dust from deserts. The Sahara desert is one of the most important dust sources on the Planet, with northern Africa being responsible for half of the global emissions of mineral dust (Middleton and Goudie, 2001; Prospero et al., 2002). In the IP, the mineral fraction of PM comes mainly from local resuspension and external contributions such as the Saharan/Sahelian dust (Querol et al., 1998, 2001; Artíñano et al., 2001; Rodríguez et al., 2001, 2002).

Urban to regional air quality models play a key roles in assessing and understanding the dynamics of air pollution, forecasting the air quality and developing emissions abatement plans and alerting the population when health-related issues occur (European Commission, 2008). Examples of air quality forecasting systems currently operating in Europe are compiled in Menut and Bessagnet (2010) and in Balk et al. (2010), the latter in the framework of the COST ES0602 action (www.chemicalweather.eu), which also complement other air quality European initiatives such as the Global Monitoring for Environment and Security (GEMS, <http://www.gmes.info/>), PROTool MOntoring for the GMEs Service Element (PROMOTE, <http://www.gse-promote.org/>) and Monitoring Atmospheric Composition and Climate (MACC, <http://www.gmes-atmosphere.eu/>). Regional air quality models are useful tools to describe the continental transport of air pollutants. However, a higher spatial resolution is required to evaluate the exposure of the population to PM pollution in urban areas, especially over complex topography such as over the IP (Jiménez et al., 2006). Up to now, there are several evaluation studies demonstrating the difficulty for models to simulate PM₁₀ and PM_{2.5} concentration over Europe (Pay et al., 2010a and references therein). Most of them deal with regional background stations, mainly from EMEP network, and quantify the model performance to reproduce regional background aerosols. Overall these show a large gap between simulated and observed PM₁₀ concentration (broadly a factor of 2) due to deficiencies in the physical and chemical understanding of the processes which lead to the formation of secondary aerosol and to the lack of accurate particulate matter emission inventories. It is worth noting that only a few published works (Hodzic et al., 2005; Flaounas et al., 2009; Chemel et al., 2010) report on performance characteristics of long-term aerosol simulations over urban domains hampered by the lack of measured PM compounds.

The CALIOPE modeling system is a state-of-the-art modeling system, specially developed with high spatial (4 km \times 4 km) and temporal resolution (1 h) to forecast air quality across Spain. The modeling system was first evaluated in Pay et al. (2010a) for Europe, and Baldasano et al. (2011) for Spain, including gas and particulate pollutants over the full year 2004. The purpose of the present paper is to complement these results by (1) providing a detailed quantitative analysis of the capabilities of the CALIOPE modeling system to simulate daily aerosol distribution over Spain in terms of concentration, size and chemical composition, and (2) estimating and assessing the spatial and seasonal distribution of the different aerosols over Spain based on comparing model outputs and observations. The study is carried out for the full year 2004 for two main reasons: (1) the HERMES emission database was compiled for this year and (2) a number of data sets on levels of PM

compounds are available for this year. An important novel approach of this work is the evaluation of the BSC-DREAM8b model using an experimental data set of African PM₁₀-dust obtained with the methodology described in Escudero et al. (2007b). In addition, measurements of chemically speciated aerosol are available in a long time series for 2004 for different environments, which allow evaluating the skill of CALIOPE to reproduce PM in urban/suburban/rural areas.

The outline of the paper is as follows. Section 2 describes the CALIOPE system and the observational data sets used for the evaluation. In Section 3, measurements of aerosol size and composition from IDAEA-CSIC/EMEP are used to identify the origin of the discrepancies in modeled aerosol and to quantify the deviation from observations. It also estimates and assesses the spatial and seasonal distribution of aerosols over Spain, for both size and composition, taking into account the discrepancies outlined in the previous section. Finally, conclusions and suggestions for further work are given in Section 4.

2. Methods

2.1. Modeling system formulation

The CALIOPE project has established an air quality forecasting system for Spain (Baldasano et al., 2008a). Current forecasts and near real-time evaluation are available through <http://www.bsc.es/calioppe>. CALIOPE encompasses a high-resolution air quality forecasting system being applied to Europe as a mother domain (12 km \times 12 km, 1 h) (Pay et al., 2010a) and Spain as the nested domain (4 km \times 4 km, 1 h) (Baldasano et al., 2011).

Meteorological input data for the chemistry transport model are calculated using the Advanced Research Weather Research and Forecasting (WRF-ARW) model v3.0.1.1 (Michalakes et al., 2004; Skamarock and Klemp, 2008). For the Spanish domain WRF-ARW is configured with a grid of 397 \times 397 points corresponding to a 4 km \times 4 km horizontal resolution and 38 σ vertical levels with 11 characterizing the planetary boundary layer (PBL). The model top is defined at 50 hPa to resolve the troposphere–stratosphere exchanges properly.

The Models-3 Community Multiscale Air Quality Modeling System (Models-3/CMAQ, Byun and Schere, 2006), is a three-dimensional Eulerian photochemical transport model that uses state-of-the-science routines to model the behavior of air pollutants from regional to local scales, due to its generalized coordinate system and its advanced nesting grid capability. CMAQ version 4.5, used in this study, has been extensively evaluated under various conditions and locations in the US (Appel et al., 2007, 2008; Roy et al., 2007), European continent (Matthias, 2008; Pay et al., 2010a), and Spain (Jiménez et al., 2006; Baldasano et al., 2011). It includes gas, aerosol and heterogeneous chemistry. According to the work by Jiménez et al. (2003) the photochemical mechanism used in this study is the Carbon Bond IV mechanism (CBM-IV, Gery et al., 1989).

The aerosols are modeled using the AERO4 module (Binkowski and Roselle, 2003). This module comprises the following aerosol compounds: nitrate, sulfate, ammonium, elemental and organic carbon (with three subcomponents: primary, secondary anthropogenic and secondary biogenic), soil, sodium, and chlorine. Unspecified anthropogenic aerosols and aerosol water are additionally kept as separate components. Aerosols are represented by three size modes (Aitken, accumulation- and coarse-mode) each of them assumed to have a lognormal distribution. The coarse particles mode is treated as dry and chemically inert with a fixed geometric standard deviation of 2.2 (Kelly et al., 2010), thus there is no dynamic interaction between the fine and coarse-mode. Secondary inorganic

aerosols (SIA) are generated by nucleation processes from their precursors to form nitrate ammonium and non-marine sulfate aerosols. The thermodynamic equilibrium between gas and inorganic fine aerosols is determined by the ISORROPIA model (Nenes et al., 1998). Secondary organic aerosol (SOA) can be formed from aromatics (anthropogenic organic aerosols) and terpenes (biogenic organic aerosols) (Schell et al., 2001). The production of sea-salt aerosol (SS) is implemented as a function of wind speed and relative humidity (Gong, 2003; Zhang et al., 2005) through the AERO4 aerosol module. Aerosol deposition is treated by a second-generation deposition velocity scheme (Binkowski and Shankar, 1995; Venkatram and Pleim, 1999). In this study simulated PM concentrations do not include the water mass and Stokes diameter are used for characterizing aerosol geometry.

Emissions are processed using the HERMES model (Baldasano et al., 2008b) specifically developed for Spain. Anthropogenic emissions are calculated by sector-specific sources or by individual installations and stacks following a bottom-up approach. Emissions are derived from the aggregation in space from 1 km × 1 km to 4 km × 4 km. According to natural biogenic emissions, HERMES calculates volatile organic compounds from vegetation as a function of temperature and photosynthetically active radiation (Guenther et al., 1995; Parra et al., 2004, 2006). Land-use categories for each grid cell are obtained from CORINE Land Cover 2000 map starting with a resolution of 100 m. In this study HERMES provides a comprehensive description of the gas-phase primary emissions speciated to the CBM-IV chemical speciation profile. The CBM-IV mechanism in CMAQv4.5 is modified from the original in Gery et al. (1989) in order to include gaseous species that are necessary to link gas-phase chemistry to aerosol formation (sulfuric acid, toluene, xylene, cresol, and monoterpenes). On the other hand, HERMES estimates PM10 and PM2.5 primary emission from anthropogenic origin, and after that it speciates fine-particles in (1) organic aerosol, (2) elemental carbon, (3) sulfate, (4) nitrate; and (5) other fine PM based on profiles in SPECIATE 3.2 (http://www.epa.gov/ttn/chief/emch/speciation/cbiv-profiles_mar_4_2002.xls), which is sector dependent. Note that HERMES quantifies PM emissions resulting from paved road resuspension (Pay et al., 2010b) which is an important feature for PM10 studies in urban air pollution (Querol et al., 2008; Amato et al., 2010).

Due to the importance of trans-boundary air pollution, HERMES also estimates emissions from Portugal and southern France using a top-down approach from the EMEP emission inventory (50 km × 50 km horizontal resolution) spatially disaggregated to 4 km × 4 km horizontal resolution.

The CMAQ horizontal grid resolution corresponds to that of WRF. Its vertical structure was obtained by a collapse from the 38 WRF layers to a total of 15 layers steadily increasing from the surface up to 50 hPa with a stronger density within the PBL. The mean altitude of the lowest layer of CMAQ in CALIOPE system is of 19.5 ± 0.5 m above ground level. Boundary and initial conditions are derived from CALIOPE-EU simulation (12 km × 12 km grid for Europe and 1 h in time) (Pay et al., 2010a).

The long-range transport of mineral dust from Sahara desert is modeled by BSC-DREAM8b (Pérez et al., 2006a,b) over the domains of study. In this framework, the model results for PM in both domains are achieved by adding the Saharan dust contribution from BSC-DREAM8bin to the CMAQ anthropogenic species over the accumulation- and coarse-modes following the work by Jiménez-Guerrero et al. (2008).

As CALIOPE is a fundamental model system, the authors wish to stress that apart from the discussion of Figs. 4, 9 and 10 and 11, neither correction factors nor any adjusting model parameterization were applied to the model output or the original model codes.

2.2. Particulate matter observations in Spain: levels and chemical speciation

The levels and chemical speciated aerosol simulated by CALIOPE are compared against observations provided by the IDAEA-CSIC (Institute of Environmental Assessment and Water Research, Spanish Research Council). They provided measurements from selected Spanish stations for the whole year 2004. Fig. 1 shows the location of the 25 stations which accomplish the objectives of spatial cover for representing most of the geographical areas in Spain and also anthropogenic activities. Thus, the selected stations are representative of the rural background, suburban background, urban background and urban-industrial background. Table 1 provides detailed characteristics of the aforementioned stations.

Besides PM10 and PM2.5 concentrations, six aerosol components are considered: total carbon (TC), sea-salt (as sum of marine sulfate, chloride and sodium), non-marine sulfate (nm-SO₄²⁻), nitrate (NO₃⁻), ammonium (NH₄⁺) and desert dust.

Measured PM10 and PM2.5 concentrations are estimated by means of the standard gravimetric method according with the Directive 1999/30/EC. Bulk acid digestion and water extraction were applied to sub-samples, as described by Querol et al. (2001). Non-mineral carbon concentrations are quantified indirectly by a CHNS elemental analyzer after subtraction of Carbon from CaCO₃, as deduced stoichiometrically from experimental Ca levels. The soluble anions (SO₄²⁻, NO₃⁻, Cl⁻) in the water extracts were quantified by ion chromatography. NH₄⁺ analyses were performed by FIA colorimetry or ion specific electrode. Marine aerosol is determined as the sum of the Na⁺ (ICP-AES) and Cl⁻ (ion chromatography).

Desert dust from Sahara is estimated by a new methodology developed by the IDAEA-CSIC (Escudero et al., 2007b) which estimates daily African PM load during dust outbreaks in southern Europe. The daily net dust load in PM10 attributable to an African episode in a given region can be obtained by subtracting the daily regional background level (RB) from the PM10 concentration value for the day with African dust outbreak at the rural station. The RB is obtained from the monthly moving 40th percentile from the PM10 time series after a prior extraction of the data of the days with African dust transport.

2.3. Evaluation methods

Modeled raw outputs are post-processed in order to be compared with quantified measured aerosols. A list of CMAQ aerosol module variables can be found in Binkowski and Roselle (2003) and the sea-salt species have been updated in CMAQv4.5 as described by Shankar et al. (2005). From these variables, fine-particles [nm-SO₄²⁻], [NO₃⁻], [NH₄⁺], [TC] are approximated by summing the appropriate Aitken- and accumulation-mode concentrations. TC is estimated by summing the modeled concentrations of primary organic aerosol, anthropogenic and biogenic secondary organic aerosol (SOA) and elemental carbon. To compare with measured PM10 sea-salt aerosol (SS), modeled sodium and chlorine (both in accumulation- and coarse-mode) and sulfate (coarse-mode) are counted in the variable SS (SS = [SS]_{fine} + [SS]_{coarse}). Modeled PM10 desert dust (DD) is estimated from BSC-DREAM8b corresponding bins ≤ 10 μm (DD = [DD]_{fine} + [DD]_{coarse}).

The BSC-DREAM8b is run offline and the outputs are then added to the CMAQ-calculated PM (Jiménez-Guerrero et al., 2008). BSC-DREAM8b used a 50 km × 50 km horizontal resolution for integrations; its outputs are interpolated to the CMAQ's Lambert conformal conic grid with a 4 km × 4 km horizontal resolution in order to add the corresponding aerosol compounds. After the interpolation, fine-particle mass is approximated by summing the modeled concentrations of all Aitken- and accumulation-mode

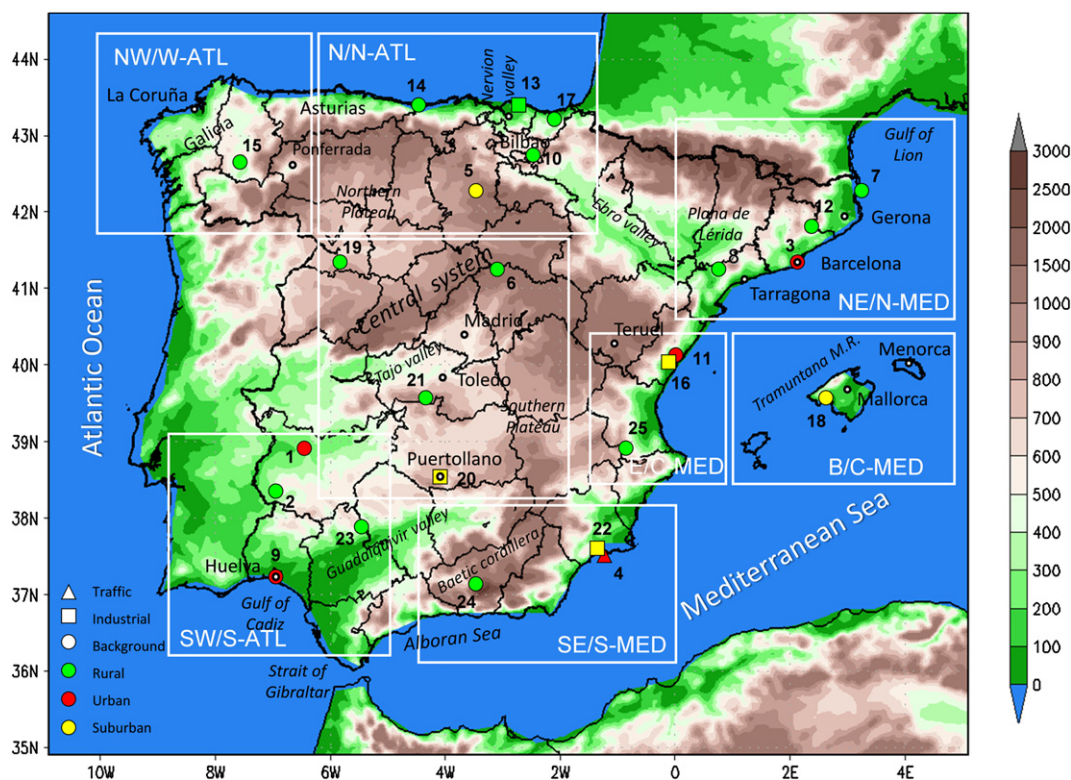


Fig. 1. Location and type of the IDAEA-CSIC and EMEP stations over Spain with data available on a daily basis in 2004. Different types of stations are represented by symbols and color codes. The various symbols represent the major emissions types affecting each station (Traffic: triangle; Industrial: square; and Background: circle) while the colors reflect the environment of each station (Urban: red; Suburban: green; and Rural: orange). The map is split in eight zones in accordance with the geographical area. Table 1 lists the main characteristics and numbers of each station. Color chart represents terrain elevation in meters. Black circles indicate place names. Names in italic show geographical systems.

species from CMAQ (PM_{i+j}) and the corresponding BSC-DREAM8b bins with diameter $\leq 2.5 \mu\text{m}$ ($[DD]_{\text{fine}}$) (Eq. (1)):

$$PM_{2.5} = [nm - SO_4^{2-}] + [NO_3^-] + [NH_4^+] + [TC] + [SS]_{\text{fine}} + [DD]_{\text{fine}} + \text{Unspeciated Mass}_{\text{fine}} \quad (1)$$

Analogously, modeled PM10 is the sum of the Aitken, accumulation- and coarse-mode ($2.5\text{--}10 \mu\text{m}$) species from CMAQ (PM_{i+j+k}) and the corresponding BSC-DREAM8b bins with diameter $\leq 10 \mu\text{m}$ (Eq. (2)):

$$PM_{10} = [PM_{2.5}] + [SS]_{\text{coarse}} + [DD]_{\text{coarse}} + \text{Unspecified Mass}_{\text{coarse}} \quad (2)$$

Note that PM_{i+j} and PM_{i+j+k} are used as an approximation of PM2.5 and PM10, respectively, since measurements (PM2.5 and PM10) are based on aerodynamic diameters and model only considers the Stokes diameter to characterize the aerosol geometry. For more detail on this issue, see Jiang et al. (2006).

It is worth mentioning that CMAQv4.5(AERO4) only estimates $nm\text{-}SO_4^{2-}$, NO_3^- , and NH_4^+ in the fine fraction. Meanwhile, calcium and sodium salts with SO_4^{2-} and NO_3^- are not taken into account, since coarse-mode is modeled as chemically inert.

Representativeness challenges continue to be present whenever gridded simulations are compared to observed data at a point in time and space as chemistry transport models simulations represent a volumetric average over an entire grid cell, meanwhile the stochastic compound embedded in the observations is not accounted for. Measurements have their own uncertainty due to biases and artifacts related to sampling and laboratory analysis methods. The European legislation (2008/50/EC) requires that the uncertainty

of PM10 and PM2.5 measurements meet the quality objective of 25%. However, legislation does not establish uncertainty criteria for chemical species yet. According to Putaud et al. (2004), inorganic species may be accurately measured with an uncertainty of about $\pm 10\%$ for major species. Consideration of uncertainties and spatial scale should be given when comparing model simulation and ambient measurements for model performance evaluation because neither one represents the absolute truth.

Hence, a variety of statistical metrics and graphic methods are used to compare the observed and modeled concentrations (Dennis et al., 2010). Besides mean and standard deviation of modeled and measured values we calculate mean bias (MB), root mean square error (RMSE), correlation coefficient (r) and the fraction of modeled concentrations that are within a factor of two and five of the measured values. We also calculate the mean fractional bias (MFB) and the mean fractional error (MFE) following the recommendation of Boylan and Russell (2006). They proposed that the model performance goal is met when both the MFE and MFB are less than or equal to 50% and $\pm 30\%$, respectively. The model performance criterion is met when both $MFE \leq 75\%$ and $MFB \pm 60\%$. These criteria and goals are selected to provide metrics for the CALIOPE performances. Since measurements are on a daily basis, aerosols are compared in terms of daily averages from the modeling system.

3. Results and discussions

The annual and seasonal statistics averaged over all studied stations based on daily values are indicated in Table 2. Scatter plots of the observed and modeled annual average concentration of each aerosol compound by station are shown in Fig. 2, where points represent the annual mean and lines indicate the 75th and 25th

Table 1
Location and characteristics of the stations for 2004.

| | Latitude ^a | Longitude ^a | Altitude (m) | Source | Station Name | Code Name | Coastal ^b | Geograp. location ^c | Type ^d | Number of data for daily concentration | | | | |
|----|-----------------------|------------------------|--------------|------------|--------------|-----------|----------------------|--------------------------------|-------------------|--|-------------|------------------------------|-----------------------|--------------------------|
| | | | | | | | | | | Total PM10 | Total PM2.5 | Speciated PM2.5 ^e | Sea-salt ^f | Desert dust ^g |
| 1 | +38.908 | -6.359 | 188 | IDAEA-CSIC | Badajoz | BAD | – | SW | UB | 363 | 363 | 58 | 52 | – |
| 2 | +38.476 | -6.923 | 393 | EMEP | Barcarrota | BAR | – | SW | RB | 343 | 343 | – | – | 106 |
| 3 | +41.385 | +2.119 | 68 | IDAEA-CSIC | Barcelona | BARC | N-MED | NE | UB | 344 | 344 | 84 | 53 | – |
| 4 | +37.604 | -0.978 | 20 | IDAEA-CSIC | Basterreche | BAS | S-MED | SE | UT | 366 | – | – | 78 | – |
| 5 | +42.335 | -3.638 | 889 | IDAEA-CSIC | Burgos | BUR | – | N | SB | 350 | 366 | 85 | 87 | – |
| 6 | +41.281 | -3.143 | 1360 | EMEP | Campisábalos | CAM | – | C | RB | 323 | 304 | – | – | 70 |
| 7 | +42.319 | +3.316 | 23 | EMEP | Cap de Creus | CAP | N-MED | NE | RB | 326 | 317 | – | – | 57 |
| 8 | +41.395 | +0.721 | 470 | EMEP | Els Torms | ELS | – | NE | RB | 341 | 336 | – | – | 65 |
| 9 | +37.270 | -6.924 | 10 | IDAEA-CSIC | Huelva | HUL | S-ATL | SW | UB | 362 | 312 | 43 | 44 | – |
| 10 | +42.653 | -2.501 | 810 | RedESP | Izki | IZK | – | N | RB | 159 | – | – | – | 39 |
| 11 | +40.074 | -0.213 | 175 | IDAEA-CSIC | L'Acora | LAC | C-MED | E | UB | 283 | 31 | – | 88 | – |
| 12 | +41.780 | +2.378 | 730 | IDAEA-CSIC | Montseny | MON | – | NE | RB | 320 | 320 | 37 | 113 | 59 |
| 13 | +43.406 | -2.704 | 116 | RedESP | Mundaka | MUN | N-ATL | N | RI | 283 | – | – | – | 35 |
| 14 | +43.439 | -4.850 | 134 | EMEP | Niembro | NIE | N-ATL | N | RB | 228 | 228 | – | – | 20 |
| 15 | +42.634 | -7.703 | 506 | EMEP | O Saviñao | OSA | W-ATL | NW | RB | 333 | 306 | – | – | 28 |
| 16 | +39.963 | -0.250 | 163 | IDAEA-CSIC | Onda | OND | C-MED | E | SI | 191 | 26 | – | 58 | – |
| 17 | +43.250 | -2.155 | 215 | RedESP | Pagoeta | PAG | N-ATL | N | RB | 283 | – | – | – | 38 |
| 18 | +39.564 | +2.623 | 117 | IDAEA-CSIC | Palma | PAL | C-MED | B | SB | 315 | – | 75 | 71 | 81 |
| 19 | +41.288 | -5.867 | 985 | EMEP | Peñaüsende | PEÑ | – | C | RB | 348 | 339 | – | – | 65 |
| 20 | +38.683 | -4.089 | 670 | IDAEA-CSIC | Puertollano | PUE | – | C | SI | 302 | – | 98 | 97 | – |
| 21 | +39.522 | -4.353 | 1241 | EMEP | Risco Llano | RIS | – | C | RB | 327 | 326 | – | – | 69 |
| 22 | +37.652 | -1.018 | 15 | IDAEA-CSIC | Santa Ana | SAN | S-MED | SE | SI | – | 323 | 83 | – | – |
| 23 | +37.996 | -5.666 | 569 | RedESP | Sierra Norte | SIE | – | SW | RB | 292 | – | – | – | 96 |
| 24 | +37.237 | -3.534 | 1230 | EMEP | Viznar | VIZ | – | SE | RB | 351 | 344 | – | – | 118 |
| 25 | +39.086 | -1.102 | 885 | EMEP | Zarra | ZAR | – | E | RB | 353 | 355 | – | – | 84 |

^a "+" is used to indicate North latitude and East longitude; "-" is used to indicate South latitude and West longitude.

^b Classification of the coastal stations according to their location: northern Mediterranean (N-MED), central Mediterranean (C-MED), southern Mediterranean (S-MED), southern Atlantic (S-ATL), northern Atlantic (N-ATL), western Atlantic (W-ATL).

^c Classification of the stations according to the geographical area: southeastern Spain (SE), southwestern Spain (SW), Balearic Islands (B), eastern Spain (E), central Spain (C), northeast Spain (NE), northern Spain (N), northwestern Spain (NW).

^d Classification of the stations according to the area type where they are located (first code: urban (U), suburban (S), and rural (R)), and according to what type of sources dominates the air pollution levels at the station (second code: traffic (T), industrial (I), and background (B)) following the specifications described in the Council Decision 97/101/EC dated January 27, 1997 (OJ L 35, 5.2.1997, p.14) and amended by Commission Decision 2001/752/EC (OJ L 282, 26.10.2001, p.69).

^e Speciated aerosol measurements corresponding to nitrate (NO₃⁻), ammonium (NH₄⁺), nm-sulfate (nm-SO₄²⁻), total carbon (TC).

^f Sea-salt aerosol (SS) indicates the speciated aerosol corresponding to the sum of sodium (Na⁺), chlorine (Cl⁻) and marine sulfate in the PM10 fraction.

^g Desert dust (DD) indicates the dust load from the Sahara desert in the PM10 fraction.

percentile distribution of observed (horizontal lines) and modeled (vertical lines) concentrations.

3.1. Evaluation of PM2.5 and PM10

A total of 18 and 24 stations are used to evaluate the simulated PM2.5 and PM10 concentrations, respectively (Table 1 and Fig. 1). For PM2.5 (PM10), 11 (15) stations are located in rural areas, 3 (4) in suburban areas, and 4 (5) in urban areas. In both cases rural background stations account for more than 50% of the number of sites (61% for PM2.5 and 58% for PM10).

Fig. 2a and b show that modeled PM2.5 and PM10 daily values are in good agreement with observations (r is 0.46 for PM2.5 and 0.59 for PM10) although modeled concentrations present a systematic negative bias. Differences in model performance for PM2.5 and PM10 are related to the major compounds in both fractions. CALIOPE's results indicate that over Spanish rural background areas carbonaceous and secondary inorganic aerosol are the major compounds in PM2.5, these account for 50–90% (30–70%) to PM2.5 (PM10), meanwhile mineral dust is the second contributor in PM10, it contributes 5–30% (10–50%) to PM2.5 (PM10). Based on correlation coefficients (Table 2), the model presents more accurate skills to reproduce the temporal evolution for PM10 than for PM2.5, which gives an indication that the main transport pattern are correctly represented by CALIOPE. In terms of normalized standard deviations, the amplitude of the daily variation is better reproduced for PM2.5 than for PM10 (0.64 vs. 0.45, respectively), especially in

summer, which suggests that modeled coarse particles daily variation seem to be too low. One source of underestimation in coarse particles is related to the fact that CMAQv4.5(AERO4) does not consider the formation of Ca(NO₃)₂ and NaNO₃ salts in the coarse fraction which are significant in Spain from mid-spring to mid-autumn (Rodríguez et al., 2002; Querol et al., 2008).

Fig. 2a and b show that the model skills are different at each site. Since all stations of the same category display similar features, the results are discussed in terms of the mean values, averaged over all rural (Fig. 3a and b), suburban (Fig. 3c and d) and urban (Fig. 3e and f) stations. For more details, time series for representative stations are shown in supplementary material Fig. S1.

Time series for PM2.5 and PM10 at rural sites show that model reproduces observations with correlation coefficients reaching 0.47 (PM2.5) and 0.65 (PM10), and with mean bias of $-5.4 \mu\text{g PM2.5 m}^{-3}$ and $-10.1 \mu\text{g PM10 m}^{-3}$. Modeled PM at urban and suburban stations presents similar performance, the correlation coefficients reach r of 0.49–0.52 (PM2.5) and 0.47–0.51 (PM10) and annual MB are around $-16 \mu\text{g PM2.5 m}^{-3}$ and $-25 \mu\text{g PM10 m}^{-3}$, in both environments. Therefore, it can be deduced that 35% (40%) of the PM2.5 (PM10) bias at urban and suburban stations is due to the underestimation of the regional background levels.

Overall, CALIOPE reproduces the observed PM daily variability along the year, with spring–summer maxima and the minimum levels in April, November and December. Modeled PM presents the best skills in summer (Table 2), when high PM levels are related to the low wet deposition (related to low humidity), low air mass

Table 2

Annual and seasonal statistics for modeled aerosol calculated at IDAEA-CSIC stations in 2004. The calculated statistics are: observed mean (OM, $\mu\text{g m}^{-3}$), modeled mean (MM, $\mu\text{g m}^{-3}$), mean bias (MB, in $\mu\text{g m}^{-3}$), correlation coefficient (r), root mean square error (RMSE, in $\mu\text{g m}^{-3}$), normalized ratio of standard deviations of the modeled mean ($\sigma(\text{Mod./Obs.})$). Data indicates the number of pairs model-observation used to calculate the statistics.

| | Data | OM | MM | MB | R | RMSE | $\sigma(\text{Mod./Obs.})$ | % within factor 2 |
|--------------------|------|------|------|-------|------|------|----------------------------|-------------------|
| PM10 | | | | | | | | |
| Annual | 7889 | 23.5 | 8.0 | -15.5 | 0.59 | 22.3 | 0.45 | 21 |
| Winter | 1949 | 20.4 | 5.4 | -15.0 | 0.52 | 23.7 | 0.24 | 18 |
| Spring | 1964 | 21.2 | 6.7 | -14.5 | 0.60 | 19.4 | 0.46 | 16 |
| Summer | 2002 | 27.8 | 11.1 | -16.7 | 0.59 | 24.6 | 0.51 | 27 |
| Fall | 1953 | 24.2 | 8.6 | -15.6 | 0.64 | 21.1 | 0.50 | 24 |
| PM2.5 | | | | | | | | |
| Annual | 5253 | 14.2 | 5.6 | -8.7 | 0.46 | 12.6 | 0.64 | 24 |
| Winter | 1255 | 14.0 | 3.6 | -10.4 | 0.55 | 15.2 | 0.29 | 16 |
| Spring | 1246 | 13.4 | 4.6 | -8.8 | 0.48 | 12.0 | 0.58 | 18 |
| Summer | 1387 | 15.7 | 7.9 | -7.8 | 0.48 | 11.6 | 0.75 | 33 |
| Fall | 1350 | 13.8 | 6.0 | -7.7 | 0.51 | 11.3 | 0.71 | 29 |
| nm-sulfate | | | | | | | | |
| Annual | 563 | 3.5 | 1.4 | -2.1 | 0.62 | 2.9 | 0.46 | 30 |
| Winter | 127 | 2.9 | 0.7 | -2.2 | 0.46 | 3.4 | 0.18 | 10 |
| Spring | 147 | 3.3 | 1.2 | -2.0 | 0.65 | 2.5 | 0.47 | 28 |
| Summer | 149 | 4.3 | 2.2 | -2.1 | 0.68 | 2.7 | 0.54 | 44 |
| Fall | 140 | 3.5 | 1.4 | -2.1 | 0.73 | 2.8 | 0.38 | 34 |
| Nitrate | | | | | | | | |
| Annual | 563 | 1.7 | 0.7 | -1.0 | 0.36 | 2.3 | 0.39 | 31 |
| Winter | 127 | 2.6 | 0.7 | -1.9 | 0.34 | 3.5 | 0.23 | 25 |
| Spring | 147 | 1.9 | 0.8 | -1.1 | 0.28 | 2.4 | 0.43 | 28 |
| Summer | 149 | 0.7 | 0.5 | -0.2 | 0.22 | 0.9 | 0.75 | 40 |
| Fall | 140 | 1.6 | 0.8 | -0.8 | 0.49 | 2.0 | 0.05 | 32 |
| Ammonium | | | | | | | | |
| Annual | 563 | 1.9 | 0.6 | -1.3 | 0.34 | 2.1 | 0.47 | 21 |
| Winter | 127 | 1.9 | 0.6 | -1.3 | 0.42 | 2.4 | 0.27 | 21 |
| Spring | 147 | 2.1 | 0.6 | -1.5 | 0.32 | 2.2 | 0.44 | 21 |
| Summer | 149 | 1.8 | 0.3 | -1.4 | 0.15 | 2.1 | 0.40 | 12 |
| Fall | 140 | 1.7 | 0.7 | -1.0 | 0.48 | 1.6 | 0.71 | 29 |
| OC+EC | | | | | | | | |
| Annual | 563 | 5.1 | 1.4 | -3.7 | 0.45 | 4.9 | 0.42 | 20 |
| Winter | 127 | 5.8 | 1.3 | -4.5 | 0.53 | 6.0 | 0.31 | 11 |
| Spring | 147 | 4.3 | 1.2 | -3.0 | 0.51 | 3.9 | 0.50 | 17 |
| Summer | 149 | 4.6 | 1.4 | -3.2 | 0.31 | 4.2 | 0.50 | 25 |
| Fall | 140 | 5.7 | 1.7 | -4.0 | 0.43 | 5.4 | 0.41 | 26 |
| Sea Salt | | | | | | | | |
| Annual | 738 | 1.2 | 0.9 | -0.3 | 0.65 | 1.2 | 1.17 | 41 |
| Winter | 153 | 1.3 | 0.9 | -0.4 | 0.70 | 1.2 | 1.14 | 34 |
| Spring | 210 | 1.3 | 1.0 | -0.3 | 0.71 | 1.2 | 1.07 | 37 |
| Summer | 193 | 1.2 | 1.1 | -0.1 | 0.52 | 1.1 | 1.44 | 47 |
| Fall | 182 | 1.2 | 0.7 | -0.4 | 0.62 | 1.1 | 1.09 | 44 |
| Desert Dust | | | | | | | | |
| Annual | 1030 | 19.4 | 13.5 | -5.9 | 0.47 | 21.9 | 0.68 | 37 |
| Winter | 88 | 14.4 | 5.3 | -9.1 | 0.18 | 30.5 | 4.45 | 16 |
| Spring | 228 | 17.0 | 8.3 | -8.7 | 0.44 | 17.9 | 0.73 | 19 |
| Summer | 409 | 22.0 | 16.9 | -5.0 | 0.45 | 26.5 | 0.61 | 43 |
| Fall | 305 | 19.2 | 15.1 | -4.1 | 0.68 | 12.9 | 1.08 | 48 |

renovation capacity due to the stable anticyclonic situation which generate recirculation episodes and accumulation in coastal areas (Baldasano et al., 1994; Millán et al., 1997), high natural resuspension of soil particles, enhanced frequency of African dust episodes and a high formation capacity of secondary aerosols by photochemical activity (Viana et al., 2002; Escudero et al., 2005). During this season the model is able to capture the amplitude of the daily variation for PM2.5 and PM10 ($\sigma(\text{Mod./Obs.}) = 0.75$ and $\sigma(\text{Mod./Obs.}) = 0.51$, respectively). Also high performances of CALIOPE are found during April, beginning November and December (Fig. 3a and b), where PM variability is attributed to the higher frequency of advection of Atlantic air masses, associated with a high rainfall rate.

However, in winter (February and ending November) the modeling system presents low skills to reproduce observation,

underestimating the amplitude of the daily variation in PM2.5 and PM10 ($0.24 < \sigma(\text{Mod./Obs.}) < 0.29$). Local anthropogenic emissions dominated high PM levels at urban and industrial sites in February 2004 (or winter 2004) when strong anticyclonic atmospheric condition (17 days) took place in the western Mediterranean Basin leading to the accumulation of PM (Pey et al., 2010). Under low dispersive conditions in February and ending November the modeling system presents the major problems.

3.2. Evaluation and assessment of PM speciation

The previous section analyzed the total concentration of PM2.5 and PM10. Although the modeling system reproduces quite well the temporal variability, systematic underestimations have been detected. It is important for these reasons to assess the modeling system ability to simulate the chemical composition of PM, not just the PM concentrations.

In the present section, we characterize the CALIOPE performance to reproduce the daily variability of the observed PM compounds (nm-SO₄²⁻, NO₃⁻, NH₄⁺, OC + EC, SS and DD) over Spain and we also estimate a multiplicative adjustment ratio for each compound. Several studies have demonstrated the benefit of adjusting site-specific air quality models using observational data to reduce systematic model error (e.g. Hogrefe et al., 2006; Djalalova et al., 2010). Bias-adjustment strategies range from the relatively simple mean bias and multiplicative ratio adjustments used by McKeen et al. (2005) to the more complex Kalman filter techniques (Delle Monache et al., 2006; Kang et al., 2010). In this study we estimate a spatial homogenous correction factor based on the ratio of annual modeled mean over measured mean. Fig. 4 displays the annual time series of the raw and corrected daily modeled concentrations for PM chemical compounds for which the estimated adjusting ratio is different to 1.

A total of 8 stations are used to evaluate the simulated nm-SO₄²⁻, NO₃⁻, NH₄⁺ and TC concentrations in the PM2.5 fraction: 1 station is located in rural areas, 4 in suburban areas and 3 in urban areas (Table 1 and Fig. 1). 75% of these stations are background stations and the other 25% are industrial. SS is evaluated over 10 stations, 3 of them are inland stations (BAD, BUR and PUE), 3 are located over < 30 km away from the coastal line (LAC, MON and OND) areas, and 4 over the coastal line (BARC, BAS, HUL and PAL). DD is available over 16 rural background stations geographically distributed over Spain.

Furthermore, the present section provides a general description of the raw CALIOPE modeled seasonal mean spatial distribution of the aerosol compounds across Spain (Figs. 6 and 7).

3.2.1. Non-marine sulfate (nm-SO₄²⁻)

On average modeled and measured nm-SO₄²⁻ concentrations present high correlation for daily concentrations ($r = 0.62$) (Fig. 2c). The modeling system reproduces 30% of the observed daily nm-SO₄²⁻ concentrations indicating that modeled nm-SO₄²⁻ is about 70% lower than observations along the trend line. At most stations, simulated annual means are underestimated by a factor of 3, with low absolute bias (MB = -2.1 $\mu\text{g m}^{-3}$). In order to examine the annual variability, Fig. 4a displays the annual time series of modeled and observed nm-SO₄²⁻ concentrations (black and red lines, respectively) on a daily basis averaged over all the stations. Modeled nm-SO₄²⁻ concentrations agree with the daily observations, especially during summer and fall ($r = 0.68$ and $r = 0.73$, respectively) (Fig. 5). In this period nm-SO₄²⁻ exhibited a maximum (Observed Mean, OM = 4.3 $\mu\text{g m}^{-3}$) because of the higher SO₂ oxidation velocity under high insolation conditions (Querol et al., 2008). Nevertheless, the modeling system tends to underestimate the peaks during February, decreasing the correlation in winter ($r = 0.46$). SO₂ presents minimum

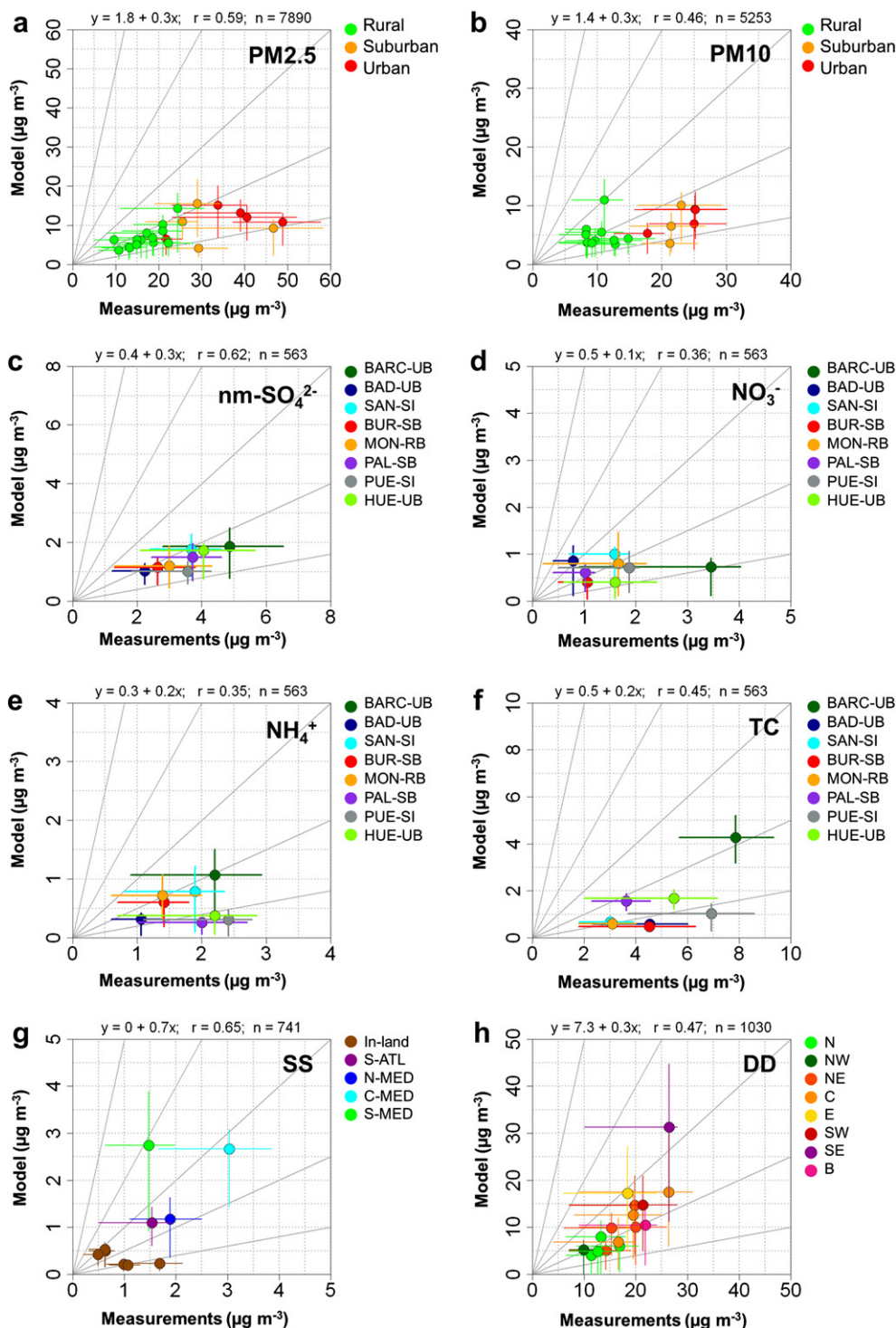


Fig. 2. Modeled vs. measured daily particulate matter (PM_{2.5} and PM₁₀) and chemically speciated aerosols (nm-SO₄²⁻, NO₃⁻, NH₄⁺, TC, SS and DD) concentrations (in µg m⁻³) by station for the year 2004. Dots represent annual average concentration in the station. Horizontal and vertical lines indicate the 25 p and 75 p, respectively. PM₁₀ (a) and PM_{2.5} (b) classifies stations as rural (green), suburban (orange) and urban (red). In c, d, e, and f each color represents a station (Fig. 1). SS (g) classifies coastal stations according to the ocean where they are located. DD (h) classifies stations according to geographic area. The expression located on the top indicates the adjust equation, the correlation coefficient (r), and the number of data points (n).

concentration in winter ($OM = 2.9 \mu\text{g m}^{-3}$) and the modeled nm-SO₄²⁻ shows the largest underestimation ($-2.2 \mu\text{g m}^{-3}$) (Table 2). Winter underestimation of nm-SO₄²⁻ is a common issue in most models in Europe, representing a direct couplet of sulfur chemistry with photochemistry, even detected with CMAQ over Europe (Matthias, 2008; Chemel et al., 2010). This feature can be explained

by the lack of model calculated oxidants or missing reactions (Kasibhatla et al., 1997; Tarrasón and Iversen, 1998; Schaap et al., 2004). After multiplying the model results by the estimated adjusting ratio (factor of 3) the corrected modeled nm-SO₄²⁻ concentrations (blue line in Fig. 4a) agree with the daily observations, especially during summer and fall.

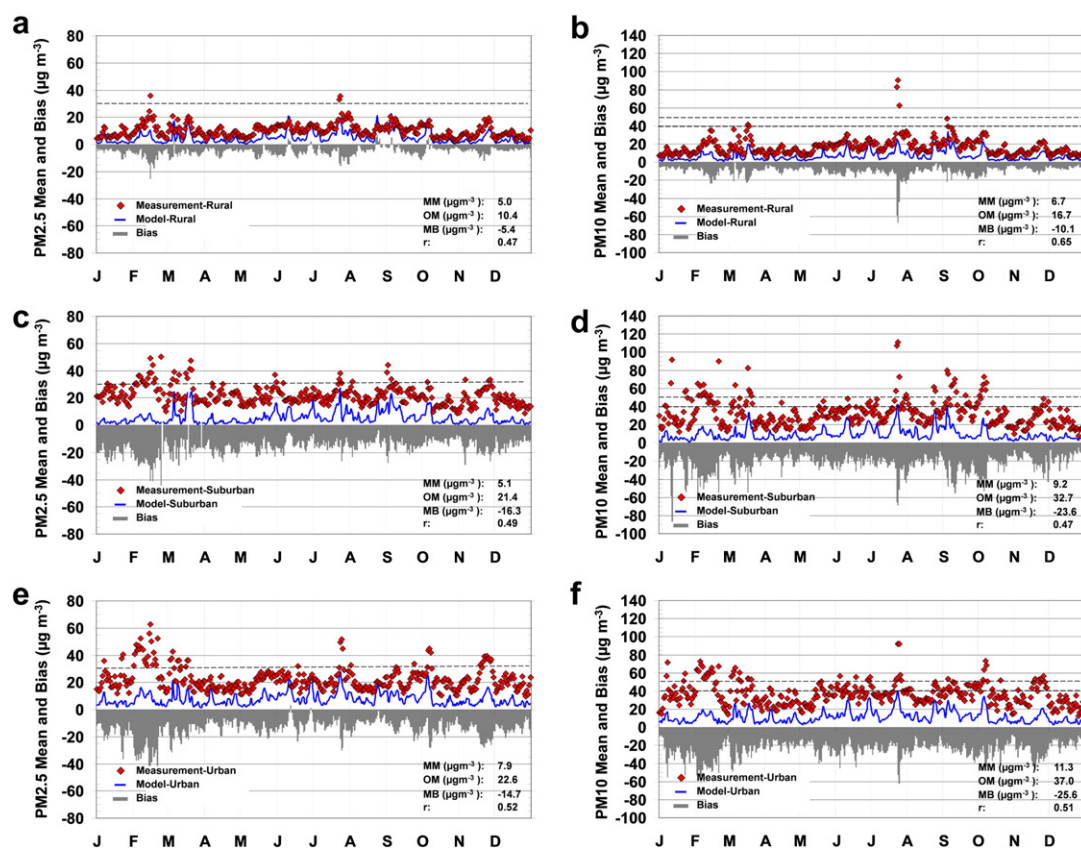


Fig. 3. Time series of observed (red diamond) and simulated (blue continuous line) daily PM_{2.5} (left column) and PM₁₀ (right column) for the year 2004 averaged over each type of site: (a, b) rural, (c, d) suburban, and (e, f) urban (Fig. 1 and Table 1 for the sites). The dashed lines represent the current limit values in Europe (European Commission, 2008) for PM₁₀ (annual and daily limit values of 40 $\mu\text{g m}^{-3}$ and 50 $\mu\text{g m}^{-3}$ not to be exceeded 35 times per year, respectively) and for PM_{2.5} (annual limit value of 25 $\mu\text{g m}^{-3}$). Statistics for each type of site are showed in the figure (bottom right): Modeled Mean (MM), Observed Mean (OM), Mean Bias (MB) and correlation coefficient (r).

Fig. 6a and b shows the seasonal mean distribution of nm-SO_4^{2-} concentration over Spain for winter and summer, respectively. nm-SO_4^{2-} concentration has lower spatial variability than other PM_{2.5} species, with significant relationship with the distribution of emission sources, mainly downwind shipping and power plants, refineries and transformation industries that are the main responsible of high concentration of SO_2 ; nm-SO_4^{2-} is mostly formed either from the gas-to-particle conversion of SO_2 in the atmosphere or from reactions in the aqueous phase. Because of the relatively slow rates of formation and removal, nm-SO_4^{2-} becomes relatively well mixed (Park et al., 2006).

Over Spain, $(\text{NH}_4)_2\text{SO}_4$ presents minimum levels in winter (Fig. 6a) and reaches maximum concentrations in summer (Fig. 6b). This seasonal pattern is related to the stronger insolation favoring the higher oxidation of SO_2 to nm-SO_4^{2-} , low air renovation at regional scale, and the increment of the summer mixing layer depth favoring the regional mixing of polluted air masses. Overall, nm-SO_4^{2-} concentrations decrease from the coast to the continent related to the fact that high-density of refineries and power plant are located near the coastal line, and also because shipping is also an important source of SO_2 .

During winter lowest concentrations ($<0.5 \mu\text{g m}^{-3}$) are detected over the main Iberian mountain ranges meanwhile winter maximum concentrations around emission sources are $\sim 1 \mu\text{g m}^{-3}$. During summer the highest concentrations are found in the Atlantic regions (northwestern Spain) ($\sim 3.5 \mu\text{g m}^{-3}$) due to the presence of geographically-close power plants, and refineries in the area of Galicia, Ponferrada, Asturias and Bilbao where SO_2 modeled level is $\sim 10 \mu\text{g m}^{-3}$, or even $50 \mu\text{g m}^{-3}$ around the La Coruña refinery.

The dispersion pattern in northwestern Spain is significantly dominated by the northern and northeastern winds oxidizing SO_2 during the transport inland. High nm-SO_4^{2-} concentrations are present along the Mediterranean coast, $\sim 2.5 \mu\text{g m}^{-3}$. Northeastern Spain is mostly affected by the Andorra power plant from Teruel (Aragón region) where nm-SO_4^{2-} is secondarily formed during the canalization of the Ebro valley toward the Mediterranean Sea. Furthermore, shipping across the Mediterranean Sea may be a cause of high nm-SO_4^{2-} along the coast. Summer nm-SO_4^{2-} is low ($\sim 1\text{--}1.5 \mu\text{g m}^{-3}$) in northern and southern plateaus corresponding with areas with low precursors emissions. The central Spanish plateau displays low levels of nm-SO_4^{2-} despite presenting one of the most important refinery and power plants around Puertollano (Castilla-La Mancha region).

Qualitative comparisons between the simulated pattern of seasonal nm-SO_4^{2-} and description based on measurements provided by Querol et al. (2008) reveals a good agreement. Such finding demonstrates the accuracy in the spatial description of the source regions and various industrial hot-spots.

Over the ocean high nm-SO_4^{2-} concentrations ($\sim 4 \mu\text{g m}^{-3}$) are located in the shipping route from the Atlantic Ocean through the Strait of Gibraltar toward the Mediterranean Sea. As indicated in Baldasano et al. (2011), ship emissions are large contributors of the total SO_2 concentrations along the ship tracks, and the subsequent formation of nm-SO_4^{2-} downwind. Maximum nm-SO_4^{2-} concentrations are in the narrow Gibraltar regions with a dispersion pattern dominated by western winds. The high nm-SO_4^{2-} in this area is a combination of high emissions from shipping, industry, power generation and oil refinery processes in the Gibraltar bay and Algeciras industrial area (Pandolfi et al., 2011).

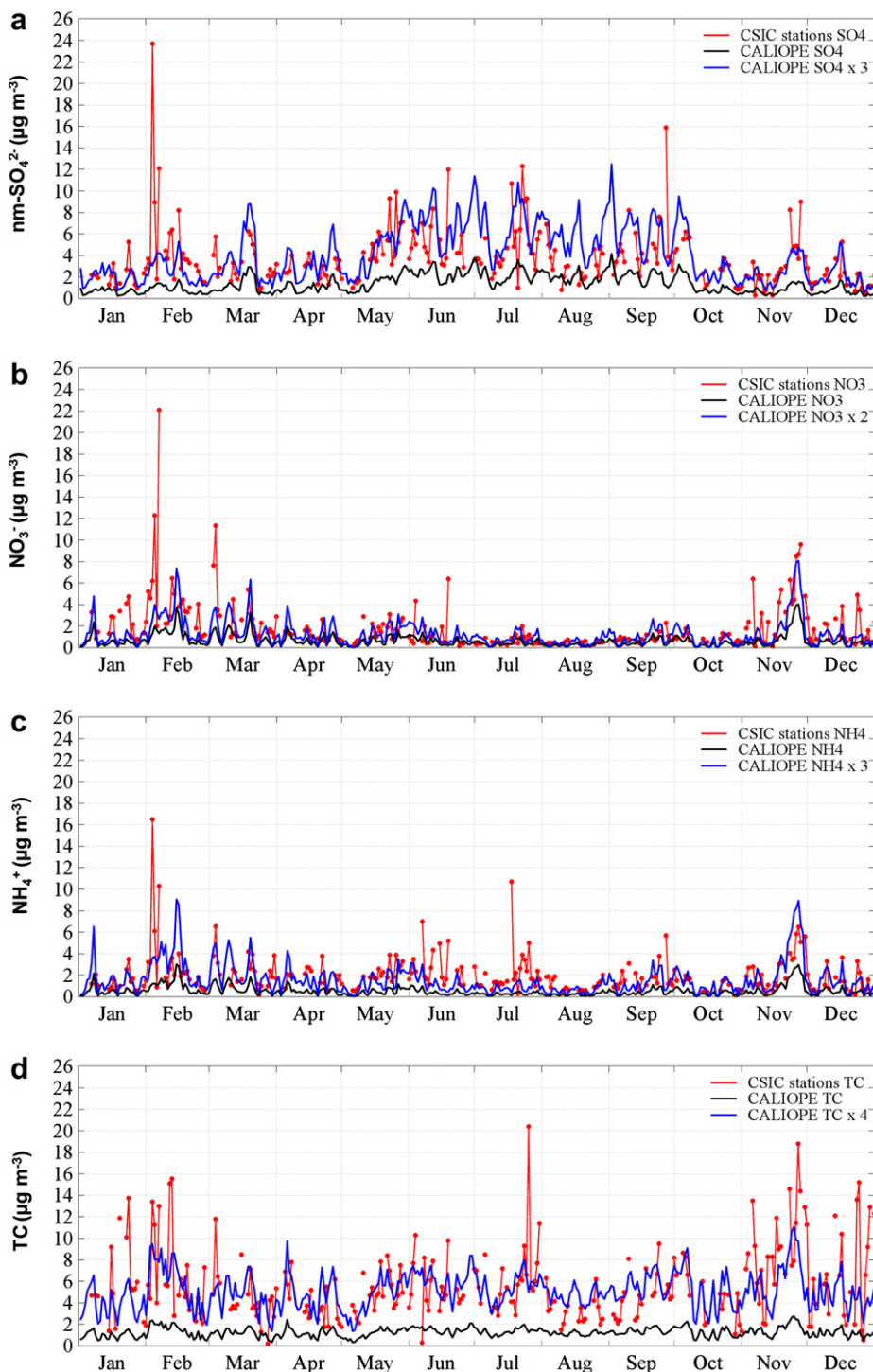


Fig. 4. Time series of observed (red lines), simulated (black line) and simulated corrected (blue line) concentration for daily nm-SO_4^{2-} (a), NO_3^- (b), NH_4^+ (c) and TC (d) as an average of all the stations for the year 2004.

3.2.2. Nitrate (NO_3^-)

Fine ammonium nitrate (NH_4NO_3) is produced by the oxidation of NO_x to nitric acid (HNO_3) during night and day (e.g. Meng et al., 1997; Nguyen and Dabdub, 2002). HNO_3 dissolves in the aqueous particles along with the ammonia (NH_3) and produces NO_3^- determined by the composition of the particle. Therefore, the behavior of nitrate is one of the most intriguing issues of inorganic atmospheric aerosols because its concentration depends not only on the amount of gas-phase HNO_3 , but also on the availability of NH_3 and nm-SO_4^{2-} ,

together with temperature and relative humidity (Mozurkewich, 1993; Nenes et al., 1998; Bassett and Seinfeld, 1983; Zhang et al., 2000; Schaap et al., 2004).

On average the CALIOPE system underestimates measured fine NO_3^- concentrations (Fig. 2d) by a factor 2 with very low bias ($\text{MB} = -1.0 \mu\text{g m}^{-3}$). The cause of this underestimation is related to errors in the simulation of NH_x ($\text{NH}_4^+ + \text{NH}_3$), SO_4^{2-} , and, to a lesser extent, TNO_3 ($\text{NO}_3^- + \text{HNO}_3$) (Yu et al., 2005). However, the temporal variability and therefore the transport patterns of NO_3^- are

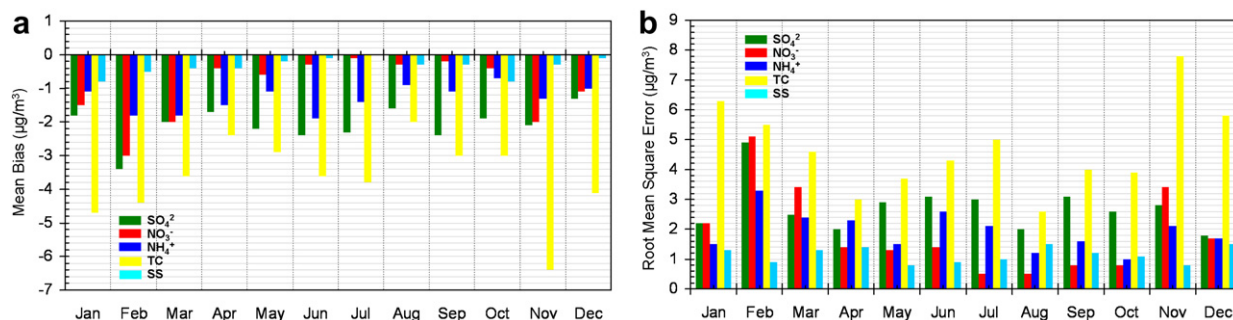


Fig. 5. Mean Bias (a, in $\mu\text{g m}^{-3}$) and Root Mean Squared Error (b, in $\mu\text{g m}^{-3}$) for nm-SO_4^{2-} (green), NO_3^- (red), NH_4^+ (dark blue), TC (yellow) and SS (cyan) averaged over the IDAEA-CSIC stations for each month of the year 2004.

captured (Fig. 4b) especially during fall ($r = 0.49$), although the modeling system hardly reproduces the amplitude of the events. Modeled NO_3^- concentrations present a good agreement with the observation when a factor of 2 is applied to the results (blue line). As for nm-SO_4^{2-} , the adapted results for NO_3^- match consistently with the observations except for February.

The seasonal mean concentration pattern of fine NO_3^- over Spain (Fig. 6c and d) shows a marked seasonal evolution characterized by a summer minimum. The oxidation rate of NO_x ranges from 5% till 50% per hour (Spicer et al., 1981) faster than that of SO_2 . Also, HNO_3 deposits rapidly and NH_4^+ presents a low thermal stability in warm season (Harrison and Pio, 1983; Querol et al., 2008). Thus, NO_3^- is spatially less homogeneously distributed than nm-SO_4^{2-} in summer as shown seasonal distribution in Fig. 6d. Levels decrease from the coastal areas to inland, with the lowest regional background levels over central and southern plateaus ($\sim 0.3 \mu\text{g m}^{-3}$).

In contrast, high NO_3^- concentration and homogeneous distributions are found in winter (Fig. 6c) favored by the higher stability of NH_4NO_3 in cool conditions, which causes a higher portion of NO_3^- to partition to the aerosol, which has a longer lifetime than HNO_3 against deposition (Schaap et al., 2004) and favored by less dispersive conditions in the boundary layer. Overall, rural background NO_3^- concentrations remain $\sim 1 \mu\text{g m}^{-3}$, reaching the lowest values in the higher mountains ranges ($< 0.5 \mu\text{g m}^{-3}$). High levels ($\sim 1.2 \mu\text{g m}^{-3}$) are found over the intensive agricultural areas of Plana de Lérida and Gerona and along the urban plume from Madrid metropolitan area which transports precursors from the agriculture and road traffic (see NH_3 and NO_2 patterns, Fig. S3, supplementary material) following a southwestern direction conditioned by the barrier of the Central System (2500 m height) and the canalization of Tajo Valley in the southern part ($\sim 1.2 \mu\text{g m}^{-3}$).

Furthermore, humidity plays a key role stabilizing NH_4NO_3 in the coasts, even at relatively high temperatures. In northeastern Spain (Galicia) there is no a significant seasonal trend of NO_3^- . Levels remain $\sim 0.9 \mu\text{g m}^{-3}$ due to the frequent Atlantic advection and the high-density industry located there. At Nervion valley, the seasonal trend of NO_3^- is smooth probably as a consequence of the significant summer breeze transport of atmospheric pollutants from the coastal industrial zones along the valley and the high humidity conditions.

Along the Mediterranean coast, the seasonal trend of NO_3^- presents low variability compared with central Spain as reported by Querol et al. (2008). The spatial difference is related to (1) the relative low disperse atmospheric condition prevailing in the Mediterranean Basin (Millán et al., 1997) compared with those in the Atlantic regions; (2) the high ammonia emission along the Mediterranean coast, above all in the northeast of Spain, caused by emission from intensive cultivation and farming (Fig. S3, supplementary material); and (3) the high humidity conditions which stabilize NH_4NO_3 even during the summer. Furthermore, traffic NH_3 emissions in urban

areas with high humidity (coastal areas) may also provoke high NH_4NO_3 levels (Athanasopoulou et al., 2008).

Thus, in contrast to nm-SO_4^{2-} , NO_3^- levels are independent of the relevance of the regional/local emission of NO_3^- precursors. This spatial distribution shows no relationship either with road traffic flows (given that cities such as Madrid and Barcelona with similar inhabitants present different NO_3^- concentrations) or with industrial density so sites with similar industrial development (Huelva and Tarragona) have very different NO_3^- levels as shown by Querol et al. (2008).

3.2.3. Ammonium (NH_4^+)

Along the year the overall variability of the modeled NH_4^+ concentrations compares favorably with observations (Figs. 2e and 5) with $r = 0.34$. As for nm-SO_4^{2-} , modeled annual mean of NH_4^+ is underestimated by a factor of 3 with very low bias ($\text{MB} = -1.3 \mu\text{g m}^{-3}$). As for NO_3^- , NH_4^+ presents the worst performance during warmer seasons ($0.15 < r < 0.32$) while is better simulated during the colder seasons ($0.42 < r < 0.48$), especially during fall season ($\sigma(\text{Mod./Obs.}) = 0.71$, $r = 0.48$). When a factor of 3 is applied the magnitude of most of the single events is captured (Fig. 4c). Similar CMAQ model results were found in Matthias (2008) and Chemel et al. (2010) where NH_4^+ concentration is underestimated in summer and the agreement with the observations is much better in winter and fall. The explanation is likely related to the uncertainties in the seasonal distribution of NH_3 emissions (Gilliland et al., 2006). There is not, to the author's knowledge, a large data set of NH_3 measurement available in Spain thus not so many conclusions can be taken over the equilibrium $\text{NO}_3^-/\text{NH}_4^+$. However, through the degree of nm-SO_4^{2-} neutralization (DON) indicator, described in the supplementary material, it is possible to provide indirectly information about how well the modeling system estimates NH_3 concentrations. $\text{PM}_{2.5} \text{ nm-SO}_4^{2-}$ is almost always completely neutralized by NH_3 in the modeling system (Fig. S2, Supplementary material). Observations suggest that $\text{PM}_{2.5} \text{ nm-SO}_4^{2-}$ is fully neutralized in warm seasons and exists in the form of NH_4^+ bisulfate in the colder months. This finding suggests that there should be more free ammonia in the gas-phase or less NH_4^+ in the photochemical model. The representation of NH_3 emissions can have a large effect on air quality model simulations of aerosol NO_3^- and NH_4^+ concentrations.

The bias performance of NH_4^+ is strongly correlated with that of nm-SO_4^{2-} ($r = 0.69$) and NO_3^- ($r = 0.62$), because both anions are neutralized by NH_4^+ . Therefore, the performance of NH_4^+ at single stations is mostly in between that of nm-SO_4^{2-} and NO_3^- . At locations where nm-SO_4^{2-} dominates over NO_3^- the performance is close to that of nm-SO_4^{2-} , whereas in regions with high modeled NH_4NO_3 the performance is closer to NO_3^- . CALIOPE performance for SIA is better for nm-SO_4^{2-} than for the other compounds based on high correlation coefficient (0.62 vs. 0.36–0.34) and normalized RMSE (0.82 vs. 1.3–1.1).

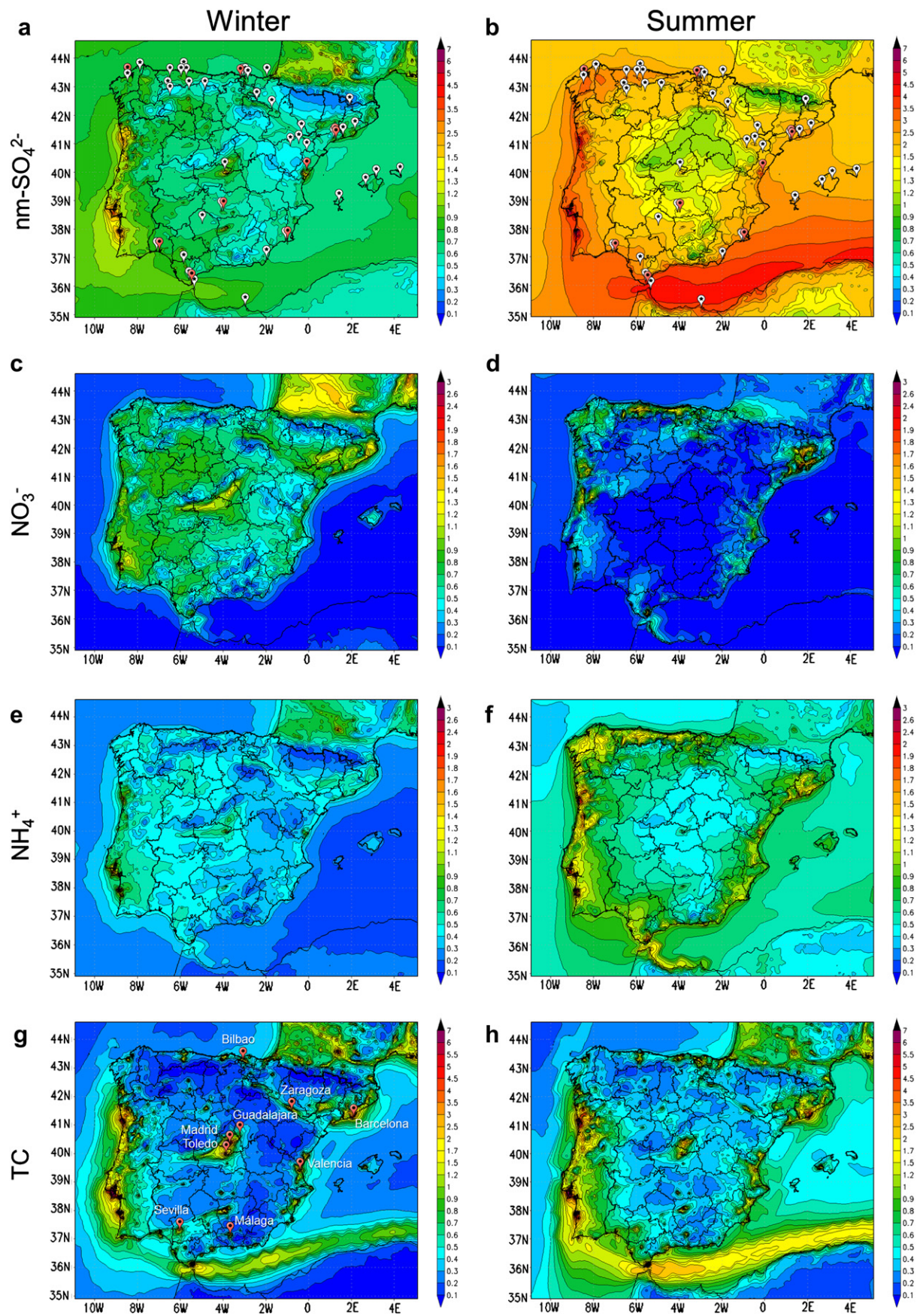


Fig. 6. Annual average concentration (in $\mu\text{g m}^{-3}$) for nm-SO_4^{2-} (a, b), NO_3^- (c, d), NH_4^+ (e, f) and TC (g, h) in winter (right) and in summer (left) at lower-most level simulated by CALIOPE over Spain at a $4\text{ km} \times 4\text{ km}$ spatial resolution. Winter corresponds to January, February and March. Summer corresponds to June, July and August. Red icons in a and b represent the Spanish refineries meanwhile white icons represent power plants.

NH_4^+ is secondarily formed as NH_3 neutralizes H_2SO_4 and HNO_3 . The amount of NH_4^+ is highly dependent on the relative amounts of H_2SO_4 and NH_3 , and indirectly of HNO_3 . The seasonal distribution pattern of NH_4^+ is shown in Fig. 6e and f for winter and summer, respectively. As for NO_3^- , the less dispersive conditions in the boundary layer favored a relative small spatial variability for NH_4^+ during winter. Average levels are $\sim 0.6 \mu\text{g m}^{-3}$, meanwhile over high mountain ranges the levels are low ($< 0.2 \mu\text{g m}^{-3}$). In summer NH_4^+ concentrations present a more complex pattern. Concentrations over the coastal areas increase ($\sim 1.2 \mu\text{g m}^{-3}$) determined by its association with nm-SO_4^{2-} . Over the Atlantic coast, northern winds determined the generation of NH_4^+ inland.

3.2.4. Total carbon (TC)

The annual temporal evolution of the modeled TC concentrations compares reasonably well with the observations ($r = 0.45$), albeit the CALIOPE system underestimates the amplitude of daily concentrations, σ (Mod./Obs.) = 0.42 (Fig. 2f and Table 2). Most measured annual mean concentrations at individual stations are underestimated by a factor of 4. These results agree with a large number of studies showing that air quality models generally underestimate organic aerosol concentrations, especially in urban air masses (Carlton et al., 2008; Murphy and Pandis, 2009; Smyth et al., 2009 among others).

The urban background station at Barcelona presents the lowest underestimation (factor of 2). In cities, a large proportion of TC is emitted by road traffic. In large conurbations ($> 500,000$ inhabitants), like Barcelona, the road traffic emission module is specifically described in HERMES, including the definition of the road network, divided in stretches (inside the $1 \text{ km} \times 1 \text{ km}$ cells), with specific temporary disaggregating profiles (distinguishing day-type: weekday-holiday, and month), average speed circulation, annual average daily traffic (number of vehicles per day), stretch length, route type (highway, road or urban) and circulation zones. Because of this complexity, the emissions at large cities are correctly described (Baldasano et al., 2008b) and hence the model tends to perform better with respect to areas with a larger uncertainty in emissions.

The TC temporal series averaged over all stations is shown in Fig. 5. The highest measured TC concentrations are found during winter ($5.8 \mu\text{g m}^{-3}$). Although the modeled TC reproduces temporal variability with high correlation ($r = 0.53$), absolute MB and RMSE are relatively weak (MB = $-4.5 \mu\text{g m}^{-3}$, RMSE = $6 \mu\text{g m}^{-3}$). On the other hand, during summer TC is modeled with the lowest correlation ($r = 0.31$), partly due to lack of SOA yield paths. The SOA model adopted in CMAQv4.5 does not include biogenic SOA formation from isoprene and sesquiterpenes (Appel et al., 2008). The predominant vegetation types in the Spanish domain favor isoprene as the main biogenic volatile organic compound (bVOC) (Keenan et al., 2009). The absence of the isoprene-SOA route on SOA modeling in the domain of study may impact significantly air quality during summer, when elevated bVOC emissions combine with an enhanced photochemistry.

The model underestimations of TC are mainly related to (1) the state-of-the-science concerning to SOA formation pathways, as commented before (Eder and Yu, 2006; Edney et al., 2007; Appel et al., 2008) and (2) probable underestimation of primary carbonaceous emission (Cooke and Wilson, 1996; Bond et al., 2004; Tsyro et al., 2007).

Fig. 6 shows the winter (g) and summer (h) mean concentration of TC over Spain in 2004. Elemental carbon is a primary pollutant so its spatial variability is relatively high. Major sources of elemental carbon include diesel engines, particulate heavy-duty trucks, and combustion process (including biomass and fossil fuel), thus high levels are associated with urban areas. In contrast, organic carbon is emitted directly or, in a large proportion, formed from the

condensation of low-volatility organic compounds. Thus, the spatial variability of organic carbon is between that of purely primary and secondary pollutants. Major primary sources of organic carbon include diesel and gasoline-burning engines, biomass burning and some industrial processes, so organic carbon will be found in urban and rural background environments.

Due to the high disaggregation and the specifically detailed emissions implemented in the HERMES model, the impact of principal highways is noticeable, (e.g. Madrid-Sevilla, Barcelona-Bilbao, the A-7 Mediterranean highway) where annual mean values range from 0.5 to $2 \mu\text{g m}^{-3}$.

In urban environment (eg. Zaragoza, Valencia, Málaga, Sevilla, Madrid and Barcelona) the seasonal trend of TC is characterized by a winter maximum (Rodríguez et al., 2002 at Barcelona site and Querol et al., 2008 at many sites), indicating a major local anthropogenic origin. Reduced dispersion conditions in the boundary layer together with enhanced condensation due to the low temperature explain the seasonal evolution of carbon in the urban environment. The urban plumes from the two largest Spanish cities (Madrid and Barcelona) reach the highest TC concentrations ($\sim 5 \mu\text{g m}^{-3}$). In both regions, on-road traffic constitutes the main source of primary pollutants in the region (Gonçalves et al., 2009) and TC follows the same pattern as NO_2 , as shown in Baldasano et al. (2011) and in Fig. S3, Supplementary material.

In Madrid during winter the TC dispersion follows a south-western direction conditioned by the barrier of Central System and the canalization of Tajo valley dominated by the predominant Atlantic advection episodes. The urban plume reaches the highest concentration at the urban nuclei ($\sim 7 \mu\text{g m}^{-3}$), moving toward Toledo (south) and reaching Guadalajara (east) to a lesser extent ($\sim 1.5 \mu\text{g m}^{-3}$). In contrast in summer, the urban plumes are less disperse, determined by the developed of the IP Thermal Low over the central plateau which couple with several deep convective cells that inject aged pollutant aloft for the Madrid area.

A different TC pattern is observed in Barcelona. The TC dispersion shows a perpendicular flow to the coast dominated by the northwestern winds. The dispersion pattern is intensified in summer due to the frequent regional recirculation events characterized by sea breeze over the Mediterranean (Baldasano et al., 1994; Millán et al., 1997). The very complex coastal terrain induces mesoscale phenomena which control the superficial wind flows. Sea-breezes and mountain valley winds contribute to the accumulation and recirculation of air masses. The littoral mountain chain (1000–1500 m height) acts as a barrier, recirculating TC flow toward the Mediterranean Sea channeled by the river valleys. Also the high isolation favors the formation of SOA.

The industrialized area of Tarragona and Castellón and the urban area of Valencia, all located along the Mediterranean coast, present significant levels of TC also affected by mesoscale phenomena dominated by sea-breezes which determine TC flow perpendicular to the coast. In northern Spain, the urban and industrial areas of Bilbao show significant TC levels dispersed along an estuary that runs almost 16 km from the center of the city to the sea and is aligned in an SE–NW direction.

In contrast, background levels of carbonaceous aerosols exhibited a light spatial variability, but a seasonal trend characterized by a summer maxima $\sim 0.5 \mu\text{g m}^{-3}$. An important fraction of SOA could arise from bVOC emissions given their increase in the warm season due to enhanced plant transpiration (Rodríguez et al., 2002; Keenan et al., 2009) and also from biomass burning from agricultural and domestic sources.

Similarly to nm-sulfate, the major shipping route originating from the northern Atlantic, toward northern Africa is shown to have a notable impact on TC concentrations, which is intensified in summer due to the increase of maritime traffic and the favored

photochemistry. Concentrations of TC range from $\sim 1.5 \mu\text{g m}^{-3}$ near the coastlines of Portugal and Gulf of Cadiz to $\sim 2 \mu\text{g m}^{-3}$ over the Alboran Sea. Background concentration of TC over the sea ranges between $\sim 0.7 \mu\text{g m}^{-3}$ and $< 0.2 \mu\text{g m}^{-3}$ over the Mediterranean and Atlantic Sea, respectively, owing to distinct Atlantic-Mediterranean regimes of Spain.

3.2.5. PM10 sea-salt aerosol (SS)

For SS, the modeling system reproduces correctly 70% of the observed values with a correctly temporal variability ($r = 0.65$) (Fig. 2g). 40% of modeled concentrations are within a factor of 2 with observations (Table 2). The modeling system presents a good skill to reproduce the amplitude of the daily variation of SS with σ (Mod./Obs.) = 1.17. Highest correlations are obtained during spring and winter when high wind velocities take place and the flux of SS is high. However, under stagnant situations, like summer over Mediterranean, the modeled sea-salt is reproduced with lower correlation and higher daily variability, $r = 0.52$ and σ (Mod./Obs.) = 1.44, respectively. As shown in Fig. 2g, at coastal stations the CALIOPE system tends to slightly overestimates SS, meanwhile at continental areas salts concentrations tends to be underestimated. Over the southern Atlantic and central Mediterranean the CALIOPE system performance agrees better with the observations. Part of the underestimation and the excessive variability modeled is because AERO4 considers coarse-mode aerosols as dry and inert. This approach does not allow important aerosol processes, such as the replacement of chloride by NO_3^- in mixed marine/urban air masses (Kelly et al., 2010) especially intense in summer when HNO_3 is

released by the thermal instability of NH_4NO_3 (Querol et al., 2004). Moreover, degassing of Cl^- is not implemented in the model, and heterogeneous reactions are not taken into account. Transfer from PM10 to PM2.5 is also not considered in AERO4. Furthermore, only sea-salt emissions from open-ocean are included so the detected underestimation over coastal areas is in part due to the fact that surf-zone mechanism is not implemented (Athanasopoulou et al., 2008). The results subscribe the modeled SS calculation performed over Mediterranean Basin in Jiménez-Guerrero et al. (2011).

Fig. 7a and b shows the non-uniform behavior of SS in the surrounding Spanish oceans, showing a strong seasonality and dependence on the wind speed variation. Over the ocean, the maximum concentrations are simulated during winter. A winter maxima of $\sim 12 \mu\text{g m}^{-3}$ is detected in the northern Atlantic Ocean and Gulf of Lion, the first related to the occurrence of intense frontal systems and strong winds events that peak during this season (Alpert and Ganor, 1993; Saaroni et al., 1998). Zakey et al. (2008) state that the Gulf of Lion is a region of strong Mediterranean cyclogenesis, with maximum activity taking place in the winter and fall months (Camuffo et al., 2000; Cavaleri, 2005). Under this condition maximum SS concentrations over the continents are found along the Atlantic coastal area of Galicia ($\sim 3 \mu\text{g m}^{-3}$) and over the whole Mallorca ($\sim 3 \mu\text{g m}^{-3}$) and Menorca ($\sim 9 \mu\text{g m}^{-3}$) islands affected by the dynamics in the Gulf of Lion. A different SS pattern is observed in summertime accentuated by the Atlantic-Mediterranean regimes. Maximum concentrations are simulated over the eastern Strait of Gibraltar ($\sim 10 \mu\text{g m}^{-3}$). The Azores high-pressure system is displaced westward and it develops high western winds which are

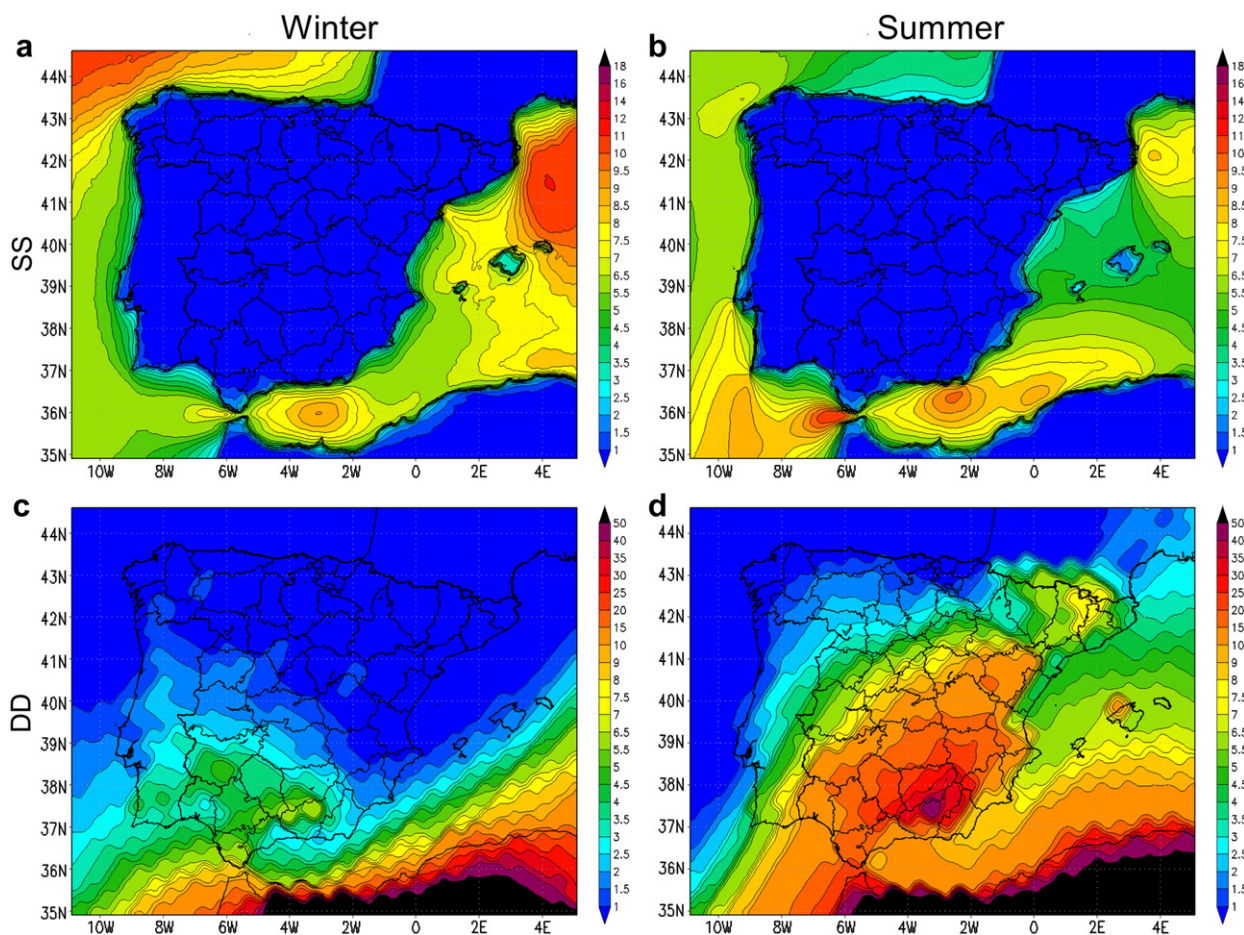


Fig. 7. Annual average concentration (in $\mu\text{g m}^{-3}$) for PM10 sea-salt aerosol (SS) (a, b), and PM10 desert dust (DD) (c, d), in winter (right) and in summer (left) at lower-most level simulated by CALIOPE over Spain at a $4 \text{ km} \times 4 \text{ km}$ spatial resolution. Winter corresponds to January, February and March. Summer corresponds to June, July and August.

intensified when they reach the strait due to its complex topography inducing SS dispersion aligned in a west to east direction (Millán et al., 2002). On the other hand, along the Mediterranean coast SS presents the maximum concentration in summer ($\sim 2 \mu\text{g m}^{-3}$) when the intensive thermal inversions, the lower convective dynamics and the low dispersive local circulations intensifies sea breeze circulation over the coast and transport SS inland.

3.2.6. PM10 desert dust (DD)

Fig. 2h presents the comparisons of the modeled DD surface concentration from BSC-DREAM8b with the DD estimated according the methodology reported by Escudero et al. (2007b). Despite the episodic character of Saharan dust outbreaks and their dependency on the synoptic scale, when BSC-DREAM8b is compared with measurements it presents a rather high correlation coefficient ($r = 0.47$) and captures the amplitude of the daily variations of desert dust episodes with high confidence, $\sigma(\text{Mod.}/\text{Obs.}) = 0.68$.

Fig. 8 shows the time series at four stations considered to be representative of the different geographical areas where Saharan dust presents a significant contribution: central (a), eastern (b), southwestern (c) and southeastern (d) Spain. BSC-DREAM8b is able to reproduce most of the Saharan dust outbreaks along the year 2004, both in time and value. Highest correlations were obtained for southeastern stations, like Víznar ($r = 0.57$), which are directly affected due to the proximity to the African continent and at high altitude. However, BSC-DREAM8b underestimates some dust events associated with meteorological situations when emissions come directly from the Atlas region. The complex orography of this region produces a mesoscale phenomenon that hampers the simulation of meteorological parameters at surface level (like winds and precipitation) and consequently, the dust emissions. The observed episode in middle March is difficult to reproduce by BSC-DREAM8b over central and southern Spain. During the 18th and 19th March, Saharan mineral dust followed an Atlantic trajectory from North Africa achieving the western part of the IP. The low Saharan dust observed before the aforementioned episode was caused by the arrival of Atlantic air masses preceding the northward high particulate flow. Another important dust event is underestimated by the BSC-DREAM8b during late July.

As shown in Fig. 7 modeled DD concentration shows a high spatial variability marked by a south-to-north gradient with minimum levels in the north ($< 2 \mu\text{g m}^{-3}$ as annual average) and maxima in the southeastern Spain ($\sim 7\text{--}9 \mu\text{g m}^{-3}$ as annual average) linked to frequent African dust plumes affecting IP (Rodríguez et al., 2001; Escudero et al., 2007b; Basart et al., 2009). These results agree with findings presented in Querol et al. (2009a). In addition, the DD contribution presents significant different patterns between winter (Fig. 8c) and summer (Fig. 8d) governed by synoptic situations as described Escudero et al. (2005). In winter African dust outbreaks were less frequent in 2004 (Fig. 8) and mainly affecting the southwestern Spain ($\sim 6 \mu\text{g m}^{-3}$) since a typical winter African transport scenario consists on the location of an anticyclone over the IP at surface levels. This creates a curved plume affecting the IP firstly on its western flank. Thus, high DD contribution during winter is found there ($\sim 5 \mu\text{g m}^{-3}$). On the other hand, in summer large amounts of DD are transported along southern and eastern Spain linked to frequent African dust outbreaks (Rodríguez et al., 2001; Escudero et al., 2005; Sicard et al., 2011; among others). Saharan dust reaches southern Spain when the north Atlantic anticyclone (Azores high) is displaced westward and the North African high is centered over Algeria (Rodríguez et al., 2001). In these episodes, DD is transported at high altitudes, between 1500 and 4000 m a.s.l (Talbot et al., 1986; Escudero et al., 2005; Pérez et al., 2004, 2006b; Olmo et al., 2008; Córdoba-Jabonero et al., 2011). The largest summer mean contribution of DD coincides with the Sierra Nevada mountain range with values reaching up to $40 \mu\text{g m}^{-3}$. Such concentrations are the consequences of (1) the mountain range location within the main zone of dust (Middleton and Goudie, 2001) and (2) the existence of several peaks within the mountain range 3000 m a.s.l. which corresponds to the altitude range for Saharan dust transport (Córdoba-Jabonero et al., 2011). In a lesser extent, summer concentration of PM10 DD load reaches concentration between 9 and $15 \mu\text{g m}^{-3}$ over southern, central and eastern Spain, including the Tramontane Mountain Range (Balearic Islands).

3.3. Modeled aerosol performance goals and criteria

Fig. 9 shows the annual MFE and MFB at each of the studied stations for PM10, PM2.5, nm-SO_4^{2-} , NO_3^- , NH_4^+ , TC, SS and DD.

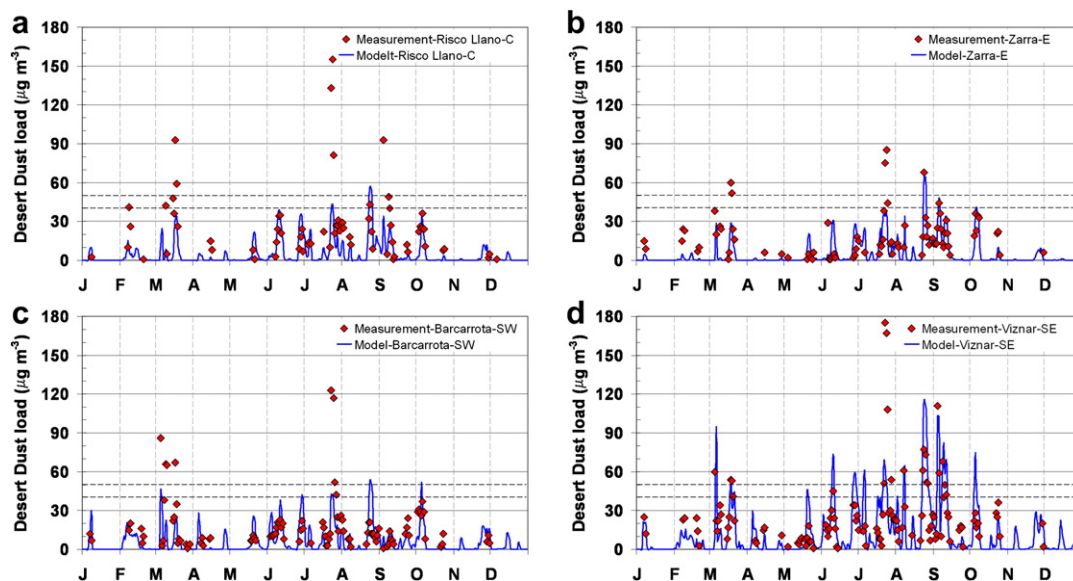


Fig. 8. Time series of observed (red diamond) and simulated (blue continuous line) daily PM10 desert dust load for the year 2004: at (a) Risco Llano, (b) Zarra, (c) Barcarrota, and (d) Víznar (Fig. 1 and Table 1 for the location of the sites). The continuous red lines represent the current limit values for PM10: the annual limit value of $40 \mu\text{g m}^{-3}$ and the daily mean value of $50 \mu\text{g m}^{-3}$ not to be exceeded 35 times in a year (European Commission, 2008).

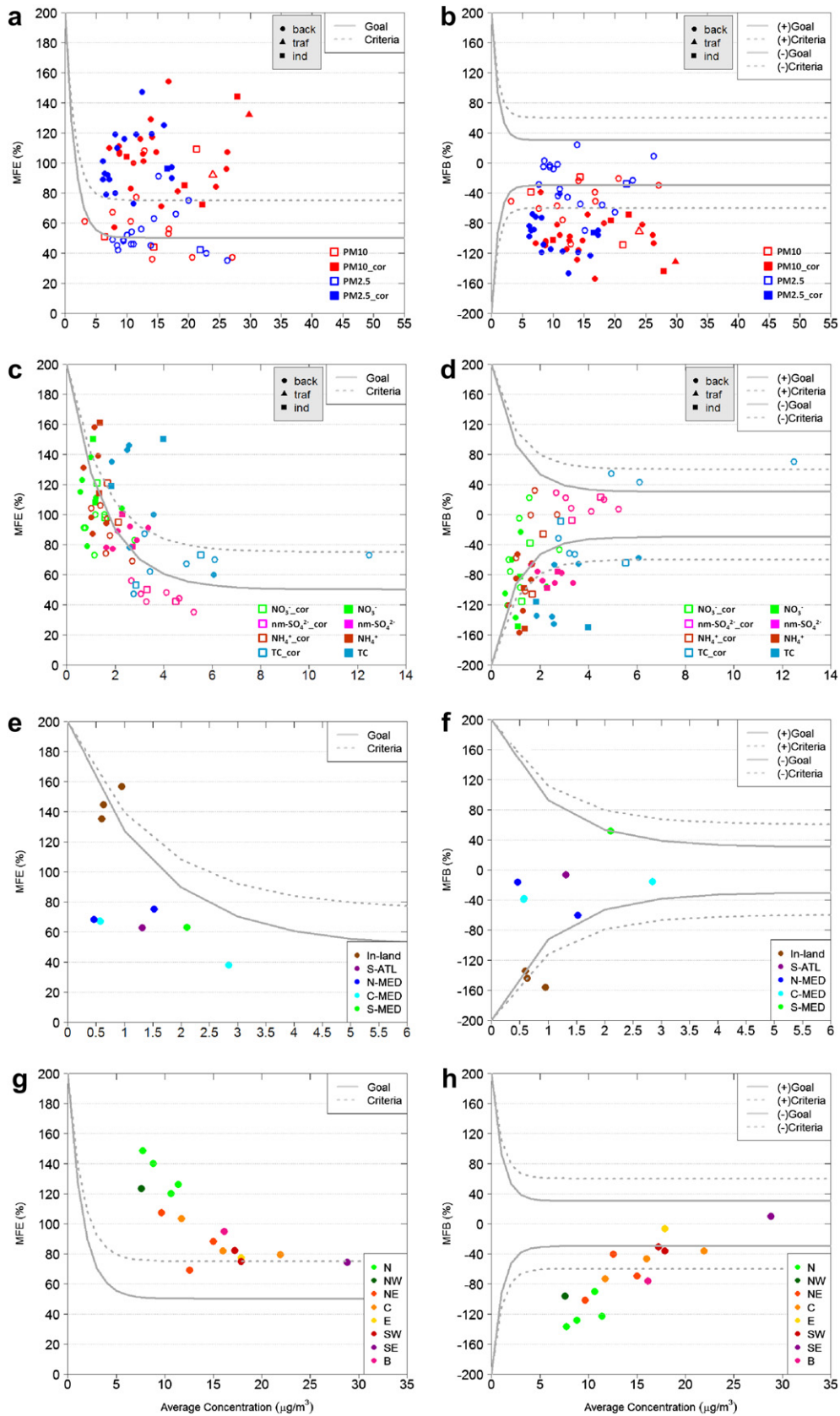


Fig. 9. Mean fractional error (MFE, left) and bias (MFB, right) by station as annual average compared to proposed performance goals and criteria by Boylan and Russell (2006). Plots are carried out for different species: PM2.5 and PM10 (a and b), nm-SO_4^{2-} , NO_3 , NH_4^+ and TC (c and d), SS (e and f) and DD (g and h). Solid symbols represent statistics for the raw modeled outputs. Empty symbols indicate corrected values calculated from the statistics evaluation. The corrected factors are 3 for nm-SO_4^{2-} , 2 for NO_3 , 3 for NH_4^+ and 4 for TC. Corrected PM2.5 and PM10 are calculated from the corrected chemical species.

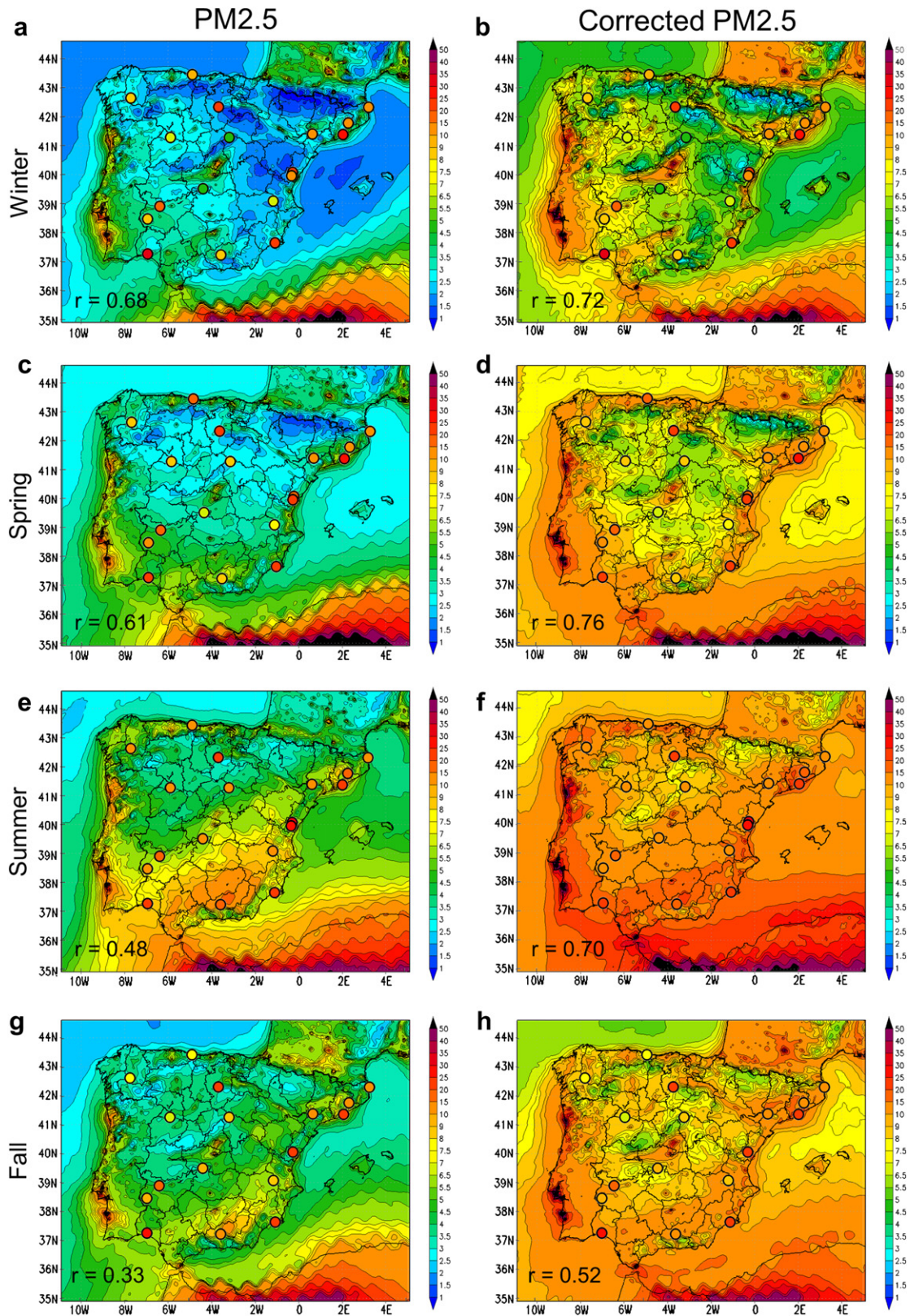


Fig. 10. Seasonal average concentrations at lower-most level ($\mu\text{g m}^{-3}$) of (left) raw modeled PM2.5 and (right) corrected PM2.5 when multiplicative correction factors are applied to nm-SO_4^{2-} , NO_3^- , NH_4^+ , and TC in the PM2.5 fraction. Seasons correspond to winter (a and b), spring (c and d), summer (e and f) and fall (g and h). Points represent measured seasonal averaged concentrations at the IDAEA-CSIC stations. The number of data points used to compute measured seasonal averaged concentrations is indicated in Table 2 in the column named Data. The number at bottom-left in each figure indicates the spatial correlation between model and observations.

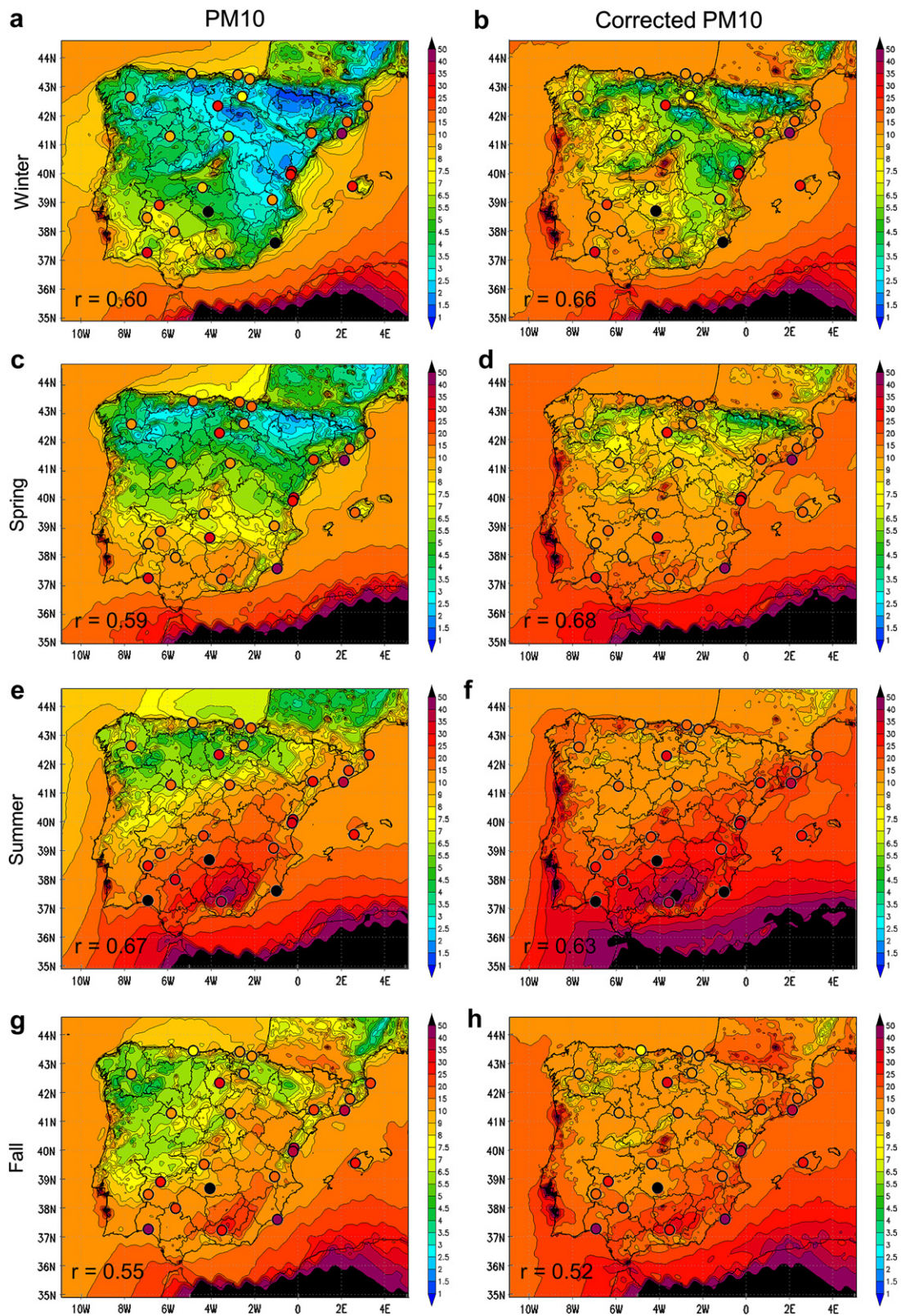


Fig. 11. Seasonal average concentrations at lower-most level ($\mu\text{g m}^{-3}$) of (left) raw modeled PM10 and (right) corrected-PM10 (right) when multiplicative correction factors are applied to nm-SO_4^{2-} , NO_3 , NH_4 , and TC in the PM2.5 fraction. Seasons correspond to winter (a and b), spring (c and d), summer (e and f) and fall (g and h). Points represent measured seasonal averaged concentrations at the IDAEA-CSIC stations. The number of data points used to compute measured seasonal averaged concentrations is indicated in Table 2 in the column named Data. The number at bottom-left in each figure indicates the spatial correlation between model and observations.

The Boylan and Russell (2006) criteria for MFB and MFE are not met for most of the stations for PM₁₀ and PM_{2.5}. Fig. 9 also shows the MFE and MFB for the aforementioned species when the multiplicative correction factors from the statistical evaluation are applied over individual species. When applied, most of the stations largely meet the model performance goals for all the species. For background stations the correction factors are effective to meet the goals although they result less effective at traffic and industrial stations.

For nm-SO₄²⁻, NO₃⁻, NH₄⁺ and TC (Fig. 9c and d) the model performance criteria for MFE is met at 21 stations out of 32. Nevertheless for MFE only 50% of the stations meet the model performance criteria. Better results are obtained for nm-SO₄²⁻ ($-100% < \text{MFB} < -90%$, $\text{MFE} < 100%$) than for NO₃⁻, NH₄⁺ and TC. The stations of Barcelona meet the criteria for MFB and MFE for OC + EC. When bias-correction factors are applied all the stations meet the criteria for MFE and MFB, and most of them meet the goals.

For SS only 8 stations out of 9 accomplished the criteria proposed by Boylan and Russell (2006). Most of the largest errors (MFE > 130%) and biases (MFB < -120%) correspond to inland stations (Fig. 9e and f). For DD (Fig. 9g and h) the central eastern and southern stations meet or nearly meet the Boylan and Russell criteria, 9 stations out of 16 corresponding to desert dust concentrations of $\sim 16 \mu\text{g m}^{-3}$. The highest MFE and MFB are found in northern and northeastern stations associated to low DD concentrations ($\sim 9 \mu\text{g m}^{-3}$).

3.4. Spatial and seasonal patterns of PM_{2.5} and PM₁₀

The present section provides a general description of the seasonal mean spatial distribution of PM size fractions (PM_{2.5} and PM₁₀) across Spain. Note that the discussion performed over PM_{2.5} and PM₁₀ takes into account the model-observations discrepancies highlighted in Sect. 3.2 for each compound by means the adjusting ratios estimated.

Fig. 10, left column, presents the seasonal mean concentration simulated with CALIOPE for PM_{2.5}. From the statistical evaluation of the chemical compounds, multiplicative bias-correction factors were estimated for nm-SO₄²⁻, NO₃⁻, NH₄⁺, and TC with the objective to reduce the annual mean bias. Fig. 10, right column, shows the modeled PM_{2.5} when the aforementioned factors are applied for each species over the whole domain. Furthermore, seasonal mean observations are also represented in both cases. In order to quantify the CALIOPE performance to reproduce the observed spatial and seasonal variability of PM_{2.5}, the spatial correlation (r) is shown bottom-left. PM₁₀ seasonal and spatial variability is discussed analogously in Fig. 11.

When the factors are applied individually to PM_{2.5} compounds, spatial correlations improve during all the seasons. The largest improvements are found in summer (from 0.48 to 0.70) associated with the increased formation of secondary aerosols, mainly nm-SO₄²⁻ and TC as shown in Sect. 3.2.4. According to PM₁₀, modeled corrected concentrations only improve correlation coefficients during winter (from 0.60 to 0.66) and spring (from 0.59 to 0.68). There is an increase in the observed PM_{2.5} and PM₁₀ levels during summertime, which is more pronounced in the coarse fraction than in the finer fraction due to the contribution of coarser size of the re-suspended dust and summer-nitrate particles (Querol et al., 2009b). The applied factors do not correct these compounds, given that coarse NO₃⁻ is not implemented in the current version of CMAQv4.5 and only re-suspended material from road traffic is included. Overall, corrected-PM₁₀ and PM_{2.5} from CALIOPE increase correlation spatially and seasonally when multiplicative correction factors for SIA and TC are applied. However, further analyses should be carried out on the coarse fraction.

Note that when the model is corrected, systematic high PM_{2.5} values ($\sim 10 \mu\text{g PM}_{2.5} \text{ m}^{-3}$) are found along the Mediterranean coast, Guadalquivir and Tajo valleys, where the impact of principal highways (Barcelona-Bilbao, the A-7 Mediterranean highway) and industrial sources (Huelva, Valencia, Tarragona) are noticeable. The highest PM_{2.5} concentrations are located around the biggest Spanish cities of Madrid and Barcelona ($> 15 \mu\text{g PM}_{2.5} \text{ m}^{-3}$). During summer PM_{2.5} background level increase, and the concentration pattern presents a low spatial variability ($\sim 10 \mu\text{g PM}_{2.5} \text{ m}^{-3}$). Similar patterns are found for corrected modeled PM₁₀, although concentrations are dominated by the DD contribution in the southern and eastern IP.

4. Conclusions

The CALIOPE system has been evaluated in terms of PM levels (PM_{2.5} and PM₁₀) and chemical compounds (nm-SO₄²⁻, NO₃⁻, NH₄⁺, TC, SS and DD) at ground level. Even more, CALIOPE annual results over the full year 2004 have been used to describe the seasonal pattern of PM and their chemical composition in Spain, increasing the knowledge on aerosol distribution.

The model performance presents wide variations among the different geographical areas in Spain. These variations also depend on the type of environment. The evaluation depicts that CALIOPE can reproduce the variability of PM_{2.5} and PM₁₀ and their main aerosols compounds over Spain ($0.45 < r < 0.64$). However, concentrations are underestimated. At urban and suburban stations PM_{2.5} and PM₁₀ levels present bias of $-15 \mu\text{g PM}_{2.5} \text{ m}^{-3}$ and $-25 \mu\text{g PM}_{10} \text{ m}^{-3}$, where 40% and 30% of these biases are due to the underestimation in the regional background concentrations.

For the first time, the BSC-DREAM8b model coupled within CALIOPE system has been evaluated in terms of DD surface concentration in the PM₁₀ fraction. The BSC-DREAM8b reproduces most of the Saharan dust outbreaks in 2004, in time and value, in areas of central, southwestern and southeastern Spain. However the BSC-DREAM8b presents difficulties to reproduce episodes where Saharan mineral dust followed an Atlantic trajectory from North Africa achieving the western IP. These later episodes are less intense than the summer ones. Concerning SS in PM₁₀, CALIOPE reproduces correctly 70% of the daily observed concentration with a correctly temporal variability. At coastal stations the modeling system tends to simulate slightly higher SS than that measured meanwhile at continental areas SS tends to be underestimated. For both natural aerosol, DD and SS, CALIOPE accomplishes the model performance criteria proposed by Boylan and Russell (2006).

The most important underestimations are linked to nm-SO₄²⁻, fine NO₃⁻, NH₄⁺ and TC. nm-SO₄²⁻ and NH₄⁺ are underestimated in a factor of 3, which is resembled in the model performance for NO₃⁻ which is underestimated in a factor of 2. Most uncertainties in the equilibrium nm-SO₄²⁻/NO₃⁻/NH₄⁺ are related to the treatment of NH₃ emission as it exhibits large spatial and temporal gradients. Annual mean concentration of TC at individual stations correlates by a factor of 4. These results agree with a large number of studies showing that air quality models generally underestimate organic aerosol concentrations, especially in urban air masses associate with uncertainties in secondary organic aerosol formation and bVOC emissions. Both temporal and spatial evaluations indicate that modeled skills for the aforementioned species improve when bias multiplicative bias-correction factors are applied over each compound. Temporally, corrected model results accomplish model performance criteria for MFB and MFE established by Boylan and Russell (2006) for each compound and total levels (PM_{2.5} and PM₁₀) at each station. Spatially, maximum improvements are found in summer for PM_{2.5} where global correlation increases from 0.48 to 0.70.

Concerning the CALIOPE results across the whole Spanish domain, PM chemical compounds exhibit geographical variations as well as marked seasonal patterns which are in agreement with the literature findings nm-SO_4^{2-} is found to be dependent mostly on the degree of industrialization of the regions. Fine NO_3^- concentration exhibits a winter maxima with no significant relationship with the distribution of emission sources, but highly dependent to the temperature and humidity. NH_4^+ spatial variability is relatively small in winter, usually being dominated by its association with nm-SO_4^{2-} . TC presents a clear winter maximum over urban environments that show its high correlation with anthropogenic emissions. SS shows a strong seasonality and dependence on the wind speed variation. Saharan air masses reach Spain when the synoptic situation is governed by depressions located to the west or southwest of the IP (winter) or when the North African anticyclone shifts to the East or Southeast of the IP (summer). DD contribution decreases from southeastern to northeastern Spain, with maximum contribution in summer ($7\text{--}30 \mu\text{g m}^{-3}$) affecting more than 50% of the Spanish country.

PM_{2.5} and PM₁₀ seasonal patterns registered maximum concentration in summer, associated with the higher frequency of African dust outbreaks, lower precipitation, higher resuspension due to soil dryness, increased formation of secondary aerosols and recirculation of air masses that prevent air renovation. Our conclusion agrees with Flaounas et al. (2009) who showed that in Mediterranean areas the use of large-scale dust emissions and transport models, such as the BSC-DREAM8b, provide more reliable PM₁₀ simulations. Furthermore, modeled annual DD contribution in Spain subscribes the measurements which estimated that the mean annual net dust contribution to the annual PM₁₀ mean recorded at rural background sites reached $< 2 \mu\text{g m}^{-3}$ in the northern Spain and $6 \mu\text{g m}^{-3}$ in the southeastern Spain (Querol et al., 2009a). On the other hand, PM₁₀ and PM_{2.5} patterns present the highest variability during winter when intense pollution episodes of either anthropogenic (winter anticyclonic scenarios) or natural (African dust) origins take place. Local pollution episodes occur mainly in these periods: the anthropogenic emission increase and the atmospheric condition favors the accumulation of pollutants around the emission sources (development of intensive thermal inversion, lower convective dynamics and low dispersive local circulations).

The results of this study suggest an increase of the spatial coverage and temporal resolution of data sets on organic and inorganic aerosols. Furthermore, measurements of gas precursor like HNO_3 , NH_3 and VOC are currently needed to test model results and identify sources of uncertainty in aerosol modeling.

The present analysis demonstrates that CALIOPE high-resolution modeling system ($4 \text{ km} \times 4 \text{ km}$, 1 h) is a useful tool which complements measurements for increasing our knowledge about PM in terms of levels and composition in (1) urban/industrial areas with a pervasive influence of anthropogenic emissions on a local scale and (2) areas with very complex terrains and meteorology like Spain. However, there are a number of possible improvements to be done in chemical transport models. Within CALIOPE, and because of the results presented here, future work should be devoted to the improvements of secondary organic aerosol formation and dynamic interactions of fine and coarse fractions by the implementation of the updated version of CMAQ (v4.7.1, aerosol module AEROS) and revision of ammonia and bVOC emission implemented in HERMES model.

Acknowledgments

The authors wish to thank the CEAM, CIEMAT and IDAEA-CSIC centers for their collaboration in the project. This work is funded by the CALIOPE project of the Spanish Ministry of the Environment

(441/2006/3-12.1, A357/2007/2-12.1, 157/PC08/3-12.0). The Spanish Ministry of Science and Innovation is also thanked for the Formación de Personal Investigador (FPI) doctoral fellowship held by María Teresa Pay (CGL2006-08903) and the Ramon y Cajal research contract hold by Pedro Jiménez-Guerrero. All simulations were performed on the MareNostrum supercomputer hosted by the Barcelona Supercomputing Center.

Appendix. Supplementary material

Supplementary data related to this article can be found online at doi:10.1016/j.atmosenv.2011.09.049.

References

- Alpert, P., Ganor, E., 1993. A jet stream associated heavy dust storm in the western Mediterranean. *J. Geophys. Res.* 98, 7339–7349. doi:10.1029/92JD01642.
- Amato, F., Nava, S., Lucarelli, F., Querol, X., Alastuey, A., Baldasano, J.M., Pandolfi, M., 2010. A comprehensive assessment of PM emissions from paved roads: real-world emission factors and intense street cleaning trials. *Sci. Total Environ.* 408, 4309–4318.
- Appel, K.W., Gilliland, A., Sarwar, G., Gilliam, R.C., 2007. Evaluation of the community multiscale air quality (CMAQ) model version 4.5: uncertainties and sensitivities impacting model performance: part I e ozone. *Atmos. Environ.* 41 (40), 9603–9613.
- Appel, K.W., Bhawe, P.V., Gilliland, A.B., Sarwar, G., Roselle, S.J., 2008. Evaluation of the community multiscale air quality (CMAQ) model version 4.5: sensitivities impacting model performance; part II e particulate matter. *Atmos. Environ.* 42 (24), 6057–6066. doi:10.1016/j.atmosenv.2008.03.036.
- Athanasopoulou, E., Tombrou, M., Pandis, S.N., Russell, A.G., 2008. The role of sea-salt emissions and heterogeneous chemistry in the air quality of polluted coastal areas. *Atmos. Chem. Phys.* 8, 5755–5769.
- Artifano, B., Querol, X., Salvador, P., Rodríguez, S., Alastuey, A., 2001. Assessment of airborne particulate matter in Spain in response to the new EU-directive. *Atmos. Environ.* 35 (1001), 43–53.
- Baldasano, J.M., Cremades, L., Soriano, C., 1994. Circulation of air pollutants over the Barcelona geographical area in summer. In: *Proceeding of 6th European Symposium Physico-Chemical Behaviour of Atmospheric Pollutants*. Verase ItalyOctober 1822Rreport EUR 15609/EN, 474–479.
- Baldasano, J.M., Jiménez-Guerrero, P., Jorba, O., Pérez, C., López, E., Güereca, P., Martín, F., García-Vivanco, M., Palomino, I., Querol, X., Pandolfi, M., Sanz, M.J., Diéguez, J.J., 2008a. CALIOPE: an operational air quality forecasting system for the Iberian Peninsula, Balearic Islands and Canary Islands- First annual evaluation and ongoing developments. *Adv. Sci. Res.* 2, 89–98.
- Baldasano, J.M., Güereca, L.P., López, E., Gassó, S., Jimenez-Guerrero, P., 2008b. Development of a high-resolution ($1 \text{ km} \times 1 \text{ km}$, 1 h) emission model for Spain: the High-Effective Resolution Modelling Emission System (HERMES). *Atmos. Environ.* 42 (31), 7215–7233.
- Baldasano, J.M., Pay, M.T., Jorba, O., Jiménez-Guerrero, P., 2011. An annual assessment of air quality with the CALIOPE modeling system over Spain. *Sci. Total Environ.* 409, 2163–2178. doi:10.1016/j.scitotenv.2011.01.041.
- Basart, S., Pérez, C., Cuevas, E., Baldasano, J.M., Gobbi, G.P., 2009. Aerosol characterization in Northern Africa, Northeastern Atlantic, Mediterranean basin and middle east from direct-sun AERONET observations. *Atmos. Chem. Phys.* 9, 8265–8282.
- Balk, T., Kukkonen, J., Karatzas, K., Bassoukos, T., Epitropou, V., 2010. A European open access chemical weather forecasting portal. *Atmos. Environ.* doi:10.1016/j.atmosenv.2010.09.058.
- Bassett, M., Seinfeld, J.H., 1983. Atmospheric equilibrium model of sulphate and nitrate aerosols. *Atmos. Environ.* 17, 2237–2252.
- Binkowski, F.S., Roselle, S.J., 2003. Models-3 community multiscale air quality (CMAQ) model aerosol component: 1. Model description. *J. Geophys. Res.* 108 (D16), 4183.
- Binkowski, F.S., Shankar, U., 1995. The regional particulate model: I. Model description and preliminary results. *J. Geophys. Res.* 100 (D12), 26191–26209.
- Boylan, J.W., Russell, A.G., 2006. PM and light extinction model performance metrics, goals, and criteria for three-dimensional air quality models. *Atmos. Environ.* 40 (26), 4946–4959.
- Bond, T.C., Streets, D.G., Yarber, K.F., Nelson, S.M., Woo, J.H., Klimont, Z., 2004. A technology-based global inventory of black and organic carbon emissions from combustion. *J. Geophys. Res.* 109, D14203. doi:10.1029/2003JD003697.
- Brauer, M., Dumayhn, T.S., Spengler, J.D., Gutschmidt, K., Heinrich, J., Wichmann, H.E., 1995. Measurement of acidic aerosol species in eastern Europe: implications for air pollution epidemiology. *Environ. Health Persp* 103, 482–488.
- Byun, D.W., Schere, K.L., 2006. Review of the governing equations, computational algorithms and other components of the models-3 community multiscale air quality (CMAQ) modeling system. *App. Mech. Rev.* 59 (2), 51–77.
- Camuffo, D., Secco, C., Brimblecombe, P., Martin-Vide, J., 2000. Sea storms in the Adriatic Sea and the western Mediterranean during the last millennium. *Clim Change* 46, 209–223. doi:10.1023/A:1005607103766.
- Carlton, A.G., Turpin, B.J., Altieri, K.E., Seitzinger, S.P., Mathur, R., Roselle, S.J., Weber, R.J., 2008. CMAQ model performance enhanced when in-cloud

- secondary organic aerosol is included: comparisons of organic carbon predictions with measurements. *Environ. Sci. Technol.* 42 (23), 8798–8802.
- Cavaleri, L., 2005. The wind and wave atlas of the Mediterranean Sea – the calibration phase. *Adv. Geosci.* 2, 255–257.
- Chemel, C., Sokhi, R.S., Yu, Y., Hayman, G.D., Vincent, K.J., Dore, A.J., Tang, Y.S., Prain, H.D., Fisher, B.E.A., 2010. Evaluation of a CMAQ simulation at high resolution over the UK for the calendar year 2003. *Atmos. Environ.* 44, 2927–2939. doi:10.1016/j.atmosenv.2010.03.029.
- Cooke, W.F., Wilson, J.J.N., 1996. A global black carbon aerosol model. *J. Geophys. Res.* 101, 19395–19409.
- Córdoba-Jabonero, C., Sorribas, M., Guerrero-Rascado, J.L., Adame, J.A., Hernández, Y., Lyamani, H., Cachorro, V., Gil, M., Alados-Arboledas, L., Cuevas, E., de la Morena, B., 2011. Synergetic monitoring of Saharan dust plumes and potential impact on surface: a case study of dust transport from Canary Islands to Iberian Peninsula. *Atmos. Chem. Phys.* 11, 3067–3091.
- Delle Monache, L., Nipen, T., Deng, X., Zhou, Y., Stull, R., 2006. Ozone ensemble forecasts: 2. A Kalman filter predictor bias correction. *J. Geophys. Res.* 110, D05308. doi:10.1029/2005JD006311.
- Dennis, R., Fox, T., Fuentes, M., Gilliland, A., Hanna, S., Hogrefe, C., Irwin, J., Rao, S.T., Scheffe, R., Schere, K., Steyn, D., Venkatram, A., 2010. A framework for evaluating regional-scale numerical photochemical modeling systems. *Environ. Fluid Mech.* 10, 471–489. doi:10.1007/s10652-009-9163-2.
- Djalalova, I., Wilczak, J., McKee, S., Grell, G., Peckham, S., Pagowski, M., Delle Monache, L., McQueen, J., Tang, Y., Lee, P., McHenry, J., Gong, W., Bouchet, V., Mathru, R., 2010. Ensemble and bias-correction techniques for air quality model forecast of surface O₃ and PM_{2.5} during the TEXAQ-S-II experiment of 2006. *Atmos. Environ.* 44, 455–467.
- Dockery, D.W., Pope III, C.A., Xu, X., Spengler, J.D., Ware, J.H., Fay, M.E., Ferris Jr., B.G., Speizer, F.E., 1993. An association between air pollution and mortality in six U.S. cities. *New Engl. J. Med.* 329, 1753–1759.
- Dueñas, C., Fernández, M.C., Cañete, S., Carretero, J., Liger, E., 2002. Assessment of ozone variations and meteorological effects in an urban area in the Mediterranean coast. *Sci. Total Environ.* 299, 97–113.
- Eder, B., Yu, S., 2006. A performance evaluation of the 2004 release of models-3 CMAQ. *Atmos. Environ.* 40, 4811–4824. doi:10.1016/j.atmosenv.2005.08.045.
- Edney, E.O., Kleindienst, T.E., Lewandowski, M., Offenber, J.H., 2007. Updated SOA Chemical Mechanism for the Community Multi-scale Air Quality Model, EPA 600/X-07/025. US Environmental Protection Agency, Research Triangle park, North Carolina.
- Escudero, M., Castillo, S., Querol, X., Avila, A., Alarcón, M., Viana, M.M., Alastuey, A., Cuevas, E., Rodríguez, S., 2005. Wet and dry African dust episodes over Eastern Spain. *J. Geophys. Res.* 110, 4731–4746.
- Escudero, M., Querol, X., Avila, A., Cuevas, E., 2007a. Origin of the exceedances of the European daily PM limit value in regional background areas in Spain. *Atmos. Environ.* 41, 730–744.
- Escudero, M., Querol, X., Pey, J., Alastuey, A., Pérez, N., Ferreira, F., Alanso, S., Rodríguez, S., Cuevas, E., 2007b. A methodology for the quantification of the net African dust load in air quality monitoring networks. *Atmos. Environ.* 41, 5516–5524.
- EEA, 2010. The European Environment. State and Outlook 2010. Air Pollution. Publication Office of the European Union, Luxembourg, ISBN 978-92-9213-152-4. doi:10.2800/57792, 46 pp.
- European Commission, 2008. Directive 2008/50/EC of the European Parliament and of the Council of 21 May 2008 on ambient air quality and cleaner air for Europe. Technical Report 2008/50/EC, L152. *Off. J. Eur. Comm.*
- Flaouas, E., Coll, I., Armengaud, A., Schmechtig, C., 2009. The representation of dust transport and missing urban sources as major issues for the simulation of PM episodes in a Mediterranean area. *Atmos. Chem. Phys.* 9, 8091–8101.
- Gery, M.W., Whitten, G.Z., Killus, J.P., Dodge, M.C., 1989. A photochemical kinetics mechanism for urban and regional scale computer modeling. *J. Geophys. Res.* 94 (D10), 12925–12956.
- Gilliland, A.B., Appel, K.W., Pinder, R.W., Dennis, R.L., 2006. Seasonal NH₃ emissions for the continental United States: inverse model estimation and evaluation. *Atmos. Environ.* 40, 4986–4998.
- Gonçalves, M., Jiménez-Guerrero, P., Baldasano, J., 2009. Contribution of atmospheric processes affecting the dynamics of air pollution in south-western Europe during a typical summertime photochemical episode. *Atmos. Chem. Phys.* 9, 849–864.
- Gong, S.L., 2003. A parameterization of sea-salt aerosol source function for sub- and super-micron particles. *J. Geophys. Res.* 108, 4107. doi:10.1029/2003GB002079.
- Guenther, A.B., Hewitt, C.N., Erickson, D., Fall, R., Geron, C., Graedel, T., et al., 1995. A global model of natural volatile organic compound emissions. *J. Geophys. Res.* 100, 8873–8892.
- Harrison, R.M., Pio, C., 1983. Sized differentiated composition of inorganic aerosol of both marine and continental polluted origin. *Atmos. Environ.* 17, 1733–1738.
- Hodzic, A., Vautard, R., Bessagnet, B., Lattuat, M., Moreto, F., 2005. Long-term urban aerosol simulation versus routine particulate matter observations. *Atmos. Environ.* 39, 5851–5864.
- Hogrefe, C., Hao, W., Civerolo, K., Ku, J.Y., Sistla, G., 2006. Exploring Approaches to Integrate Observations and CMAQ Simulations for Improved Air Quality Forecast Presented at the 5th annual CMAQ User's Conference, Chapel Hill, NC. Available: http://www.cmascenter.org/conference/2006/abstracts/hogrefe_session3.pdf.
- Hyslop, N.P., White, W.H., 2008. An evaluation of interagency monitoring of protected visual environments (IMPROVE) collocated precision and uncertainty estimates. *Atmos. Environ.* 42, 2691–2705. doi:10.1016/j.atmosenv.2007.06.053.
- IPCC, Intergovernmental Panel on Climate Change, 2007. Climate Change 2007. Synthesis Report. <http://www.ipcc.ch/pdf/assessment-report/ar4/syr/ar4syr.pdf>.
- Jacobson, M.Z., 2001. Global direct radiative forcing due to multicomponent anthropogenic and natural aerosols. *J. Geophys. Res.* 106 (D2), 1551–1568. doi:10.1029/2000JD900514.
- Jiang, W., Smyth, S., Giroux, E., Roth, H., Yin, D., 2006. Differences between CMAQ fine model particles and PM_{2.5} concentrations and their impact on model performance evaluation in the lower Fraser Valley. *Atmos. Environ.* 40, 4973–4985.
- Jiménez, P., Baldasano, J.M., Dabdub, D., 2003. Comparison of photochemical mechanisms for air quality modeling. *Atmos. Environ.* 37 (30), 4179–4194. doi:10.1016/S1352-2310(03)00567-3.
- Jiménez, P., Lelieveld, J., Baldasano, J.M., 2006. Multi-scale modeling of air pollutant dynamics in the northwestern Mediterranean basin during a typical summertime episode. *J. Geophys. Res.* 111, 1–21. doi:10.1029/2005JD006516.
- Jiménez-Guerrero, P., Pérez, C., Jorba, O., Baldasano, J.M., 2008. Contribution of Saharan dust in an integrated air quality system and its on-line assessment. *J. Geophys. Res. Lett.* 35, L03814. doi:10.1029/2007GL031580.
- Jiménez-Guerrero, P., Jorba, O., Pay, M.T., Montávez, J.P., Jerez, S., Gómez-Navarro, J.J., Baldasano, J.M., 2011. Comparison of two different sea-salt aerosol schemes as implemented in air quality models applied to the Mediterranean Basin. *Atmos. Chem. Phys.* 11, 4833–4850. doi:10.5194/acp-11-4833-2011.
- Kang, D., Mathur, R., Rao, S.T., 2010. Real-time bias-adjusted O₃ and PM_{2.5} air quality index forecast and their performance evaluations over the continental United States. *Atmos. Environ.* 44, 2203–2212.
- Kasibhatla, P., Chameides, W.L., Jonn, J.S., 1997. A three dimensional global model investigation of seasonal variations in the atmospheric burden of anthropogenic sulphate aerosols. *J. Geophys. Res.* 102, 3737–3759.
- Kelly, J.T., Bhavsar, P.V., Nolte, C.G., Shankar, U., Foley, K.M., 2010. Simulating emission and chemical evolution of coarse sea-salt particles in the Community Multiscale Air Quality (CMAQ) model. *Geosci. Model. Dev.* 3, 257–273.
- Keenan, T., Niinemets, U., Sabate, S., Gracia, C., Peñuelas, P., 2009. Process based inventory of isoprenoid emissions from European forests: model comparisons, current knowledge and uncertainties. *Atmos. Chem. Phys.* 9, 4053–4076.
- Linares, C., Díaz, J., 2010a. Short-term effect of PM_{2.5} on daily hospital admissions in Madrid (2003–2005). *Int. J. Environ. Health Res.* 20, 129–140.
- Linares, C., Díaz, J., 2010b. Short-term effect of concentrations of fine particulate matter on hospital admissions due to cardiovascular and respiratory causes among the over-75 age group in Madrid, Spain. *Public Health* 124, 28–36.
- Lovett, G., Martin, M., Traynor, M., Pouyat, R., Carreiro, M., Zhu, W., Baxter, J., 2000. Atmospheric deposition to Oak forests along an urban–rural gradient. *Environ. Sci. Technol.* 34, 4294–4300. doi:10.1021/es001077q.
- Maté, T., Guaita, R., Pichiule, M., Linares, C., Díaz, J., 2010. Short-term effect of fine particulate matter (PM_{2.5}) on daily mortality due to diseases of the circulatory system in Madrid (Spain). *Atmos. Environ.* 40, 5750–5757.
- Matthias, V., 2008. The aerosol distribution in Europe derived with the community multiscale air quality (CMAQ) model: comparison to near surface in situ and sunphotometer measurements. *Atmos. Chem. Phys.* 8, 5077–5097.
- McKee, S., Wilczak, J., Grell, G., Djalalova, I., Peckham, S., Hsie, E.Y., Gong, W., Bouchet, V., Menard, S., Moffett, R., McHenry, J., McQueen, J., Tang, Y., Carmichael, G., Pagowski, M., Chan, A.C., Dye, T.S., Frost, G., Lee, P., Mathur, R., 2005. Assessment of an ensemble of seven real-time ozone forecast over eastern North America during the summer of 2004. *J. Geophys. Res.* 110, D21307.
- Meng, Z., Dabdub, D., Seinfeld, J.H., 1997. Chemical coupling between atmospheric ozone and particulate matter. *Science* 277, 116–119.
- Menuet, L., Bessagnet, B., 2010. Atmospheric composition forecasting in Europe. *Ann. Geophys.* 28, 61–74.
- Michalakes, J., Dudhia, J., Gill, D., Henderson, T., Klemp, J., Skamarock, W., Wang, W., 2004. The weather research and forecast model: software architecture and performance. In: Mozdzynski, E.G. (Ed.), To Appear in Proceeding of the Eleventh ECMWF Workshop on the Use of High Performance Computing in Meteorology, 25–29 October 2004. Reading, U.K., pp. 117–124.
- Middleton, N.J., Goudie, A.S., 2001. Saharan dust: sources and trajectories. *Trans. Inst. Br. Geogr.* 26, 165.
- Millán, M., Salvador, R., Mantilla, E., Kallos, G., 1997. Photo-oxidant dynamics in the Mediterranean basin in summer: results from European research projects. *J. Geophys. Res.* 102, 8811–8823.
- Millán, M.M., Sanz, M.J., Salvador, R., Mantilla, E., 2002. Atmospheric dynamics and ozone cycles related to nitrogen deposition in the western Mediterranean. *Environ. Pollut.* 118, 167–186. doi:10.1016/S0269-7491(01)00311-6.
- Mozurkewich, M., 1993. The dissociation constant of ammonium nitrate and its dependence on temperature, relative humidity and particle size. *Atmos. Environ.* 27, 261–270.
- Murphy, B.N., Pandis, S.N., 2009. Simulating the formation of semivolatile primary and secondary aerosol in a regional chemical transport model. *Environ. Sci. Technol.* 43, 4722–4728.
- Nenes, A., Piliinis, C., Pandis, S.N., 1998. ISORROPIA: a new thermodynamic equilibrium model for multiphase multicomponent inorganic aerosols. *Aquat. Geochem.* 4 (1), 123–152. doi:10.1023/A:1009604003981.
- Nguyen, K., Dabdub, D., 2002. NO_x and VOC control and its effects on the formation of aerosols. *Aerosol Sci. Tech.* 36, 560–572.
- Olmo, F.J., Quitantes, A., Lara, V., Lyamani, H., Alados-Arboledas, L., 2008. Aerosol optical properties assessed by an inversion method using the solar principal plane for non-spherical particles. *J. Quant. Spectrosc. Ra* 109, 1504–1516.
- Pandolfi, M., Gonzalez-Castanedo, Y., Alastuey, A., de la Rosa, J.D., Mantilla, E., de la Campa, A.S., Querol, X., Pey, J., Amato, F., Moreno, T., 2011. Source apportionment of PM₁₀ and PM_{2.5} at multiple sites in the strait of Gibraltar by PMF: impact of shipping emissions. *Environ. Sci. Pollut. Res.* 18, 260–269.

- Park, S.K., Cobb, C.E., Wade, K., Mulholland, J., Hu, Y., Russell, A.G., 2006. Uncertainty in air quality model evaluation for particulate matter due to spatial variations in pollutant concentrations. *Atmos. Environ.* 40, S563–S573.
- Parra, R., Gassó, S., Baldasano, J.M., 2004. Estimating the biogenic emissions of non-methane volatile organic compounds from the North Western Mediterranean vegetation of Catalonia, Spain. *Sci. Total Environ.* 329, 241–251.
- Parra, R., Jiménez, P., Baldasano, J.M., 2006. Development of the high spatial resolution EMICAT2000 emission model for air pollutants from the north-eastern Iberian Peninsula (Catalonia, Spain). *Environ. Pollut.* 140, 200–219.
- Pay, M.T., Piot, M., Jorba, O., Basart, S., Gassó, S., Jiménez-Guerrero, P., Gonçalves, M., Dabdub, D., Baldasano, J.M., 2010a. A full year evaluation of the CALIOPE-EU air quality system in Europe for 2004: a model study. *Atmos. Environ.* 44, 3322–3342. doi:10.1016/j.atmosenv.2010.050140.
- Pay, M.T., Jiménez-Guerrero, P., Baldasano, J.M., 2010b. Implementation of resuspension from paved roads for the improvement of CALIOPE air quality system in Spain. *Atmos. Environ.* 45, 802–807. doi:10.1016/j.atmosenv.2010.10.032.
- Pérez, C., Sicard, M., Jorba, O., Comerón, A., Baldasano, J.M., 2004. Summertime re-circulations of air pollutants over the north-eastern Iberian coast observed from systematic EARLINET lidar measurements in Barcelona. *Atmos. Environ.* 38, 3983–4000.
- Pérez, C., Nickovic, N., Pejanovic, G., Baldasano, J.M., Özsoy, E., 2006a. Interactive dust-radiation modeling: a step to improve weather forecast. *J. Geophys. Res.* 111, D16206. doi:10.1029/2005JD006717.
- Pérez, C., Nickovic, S., Baldasano, J.M., Sicard, M., Rocadenbosh, F., Cachorro, V.E., 2006b. A long Saharan dust event over the Western Mediterranean: lidar, sun photometer observation and regional dust modeling. *J. Geophys. Res.* 111, D15214. doi:10.1029/2005JD006579.
- Pérez, L., Medina-Ramón, M., Künzli, N., Alastuey, A., Pey, J., Pérez, N., Garcia, R., Tobias, A., Querol, X., Sunyer, J., 2009. Size fractionate particulate matter, vehicle traffic, and case-specific daily mortality in Barcelona, Spain. *Environ. Sci. Technol.* 43, 4707–4714.
- Pey, J., Pérez, N., Querol, X., Alastuey, A., Cusack, M., Reche, C., 2010. Intense winter atmospheric pollution episodes affecting the Western Mediterranean. *Sci. Total Environ.* 408, 1951–1959.
- Pope III, C.A., Burnett, R.T., Thun, M.J., Calle, E.E., Krewski, D., Ito, K., Thurston, G.D., 2002. Lung cancer, cardiopulmonary mortality, and long-term exposure to fine particulate air pollution. *J. Am. Med. Assoc.* 287, 1132–1141.
- Prospero, J.M., Ginoux, P., Torres, O., Nicholson, S.E., Gill, T.E., 2002. Environmental characterization of global sources of atmospheric soil dust identified with the nimbus 7 total ozone mapping spectrometer (TOMS) absorbing aerosol product. *Rev. Geophys.* 40, 1002. doi:10.1029/2000RF000095.
- Putaud, J.-P., Raes, F., van Dingenen, R., Brüggemann, E., Facchini, M.-C., Decesari, S., Fuzzi, S., Gehrige, R., Hüglin, C., Laj, P., Lorbeer, G., Maenhaut, W., Mihalopoulos, N., Müller, K., Querol, X., Rodríguez, S., Schneider, J., Spindler, G., ten Brink, H., Torsenth, K., Wiedensohler, A., 2004. A European aerosol phenomenology-2: chemical characteristics of particulate matter at kerbside, urban, rural and background sites in Europe. *Atmos. Environ.* 38, 2579–2595.
- Querol, X., Alastuey, A., Puigercus, J.A., Mantilla, E., Miro, J.V., Lopez-Soler, A., Plana, F., Artiñano, B., 1998. Seasonal evolution of suspended particles around a large coal-fired power station: particulate levels and sources. *Atmos. Environ.* 32, 1963–1978.
- Querol, X., Alastuey, A., Rodríguez, S., Plana, F., Ruiz, C.R., Cots, N., Massagué, G., Puig, O., 2001. PM10 and PM2.5 source apportionment in the Barcelona Metropolitan Area, Catalonia, Spain. *Atmos. Environ.* 35, 6407–6419.
- Querol, X., Alastuey, A., Rodríguez, S., Viana, M.M., Artiñano, B., Salvador, P., Mantilla, E., García de Santos, S., Fernandez Patier, R., de la Rosa, J., Sanchez de la Campa, A., Menéndez, M., Gil, J.J., et al., 2004. Levels of particulate matter in rural, urban and industrial sites in Spain. *Sci. Total Environ.* 334–335, 359–376.
- Querol, X., Alastuey, A., Moreno, T., Viana, M.M., Castillo, S., Pey, J., Rodríguez, S., Artiñano, B., Salvador, P., Sánchez, M., García Dos Santos, S., Herce Garraleta, M.D., Fernandez-Patier, S., Mereno-Gau, S., Negral, L., Minguillón, M.C., Monfort, E., Sanz, M.J., Palomo-Marín, R., Pinilla-Gil, E., Cuevas, E., de la Rosa, J., Sánchez de la Campa, A., 2008. Spatial and temporal variations in airborne particulate matter (PM10 and PM2.5) across Spain 1999–2005. *Atmos. Environ.* 42, 3964–3979.
- Querol, X., Pey, J., Pandolfi, M., Alastuey, A., Cusack, M., Pérez, N., Moreno, T., Viana, M., Mihalopoulos, N., Kallos, G., Kleanthous, S., 2009a. African dust contributions to mean ambient PM10 mass-levels across the Mediterranean Basin. *Atmos. Environ.* 43, 4266–4277.
- Querol, X., Alastuey, A., Pey, J., Cusack, M., Pérez, N., Mihalopoulos, N., Theodosi, C., Gerasopoulos, E., Kubilay, N., Koçak, M., 2009b. Variability in regional background aerosols within the Mediterranean. *Atmos. Chem. Phys.* 9, 4575–4591.
- Ramanathan, V., Crutzen, P.J., Kiehl, J.T., Rosenfeld, D., 2001. Aerosols, climate, and the hydrological cycle. *Science* 294 (5549), 2119–2124. doi:10.1126/science.1064034.
- Ribas, A., Peñuelas, J., 2004. Temporal patterns of surface ozone levels in different habitats of the North Western Mediterranean basin. *Atmos. Environ.* 38, 985–992.
- Rodríguez, S., Querol, X., Alastuey, A., Kallos, G., Kakaliagou, O., 2001. Saharan dust contribution to PM10 and TSP levels in Southern and Eastern Spain. *Atmos. Environ.* 35 (14), 2433–2447.
- Rodríguez, S., Querol, X., Alastuey, A., Plana, F., 2002. Sources and processes affecting levels and composition of atmospheric aerosol in the Western Mediterranean. *J. Geophys. Res.* 107 (D24), 4777.
- Roy, B., Mathur, R., Gilliland, A.B., Howard, S.C., 2007. A comparison of CMAQ-based aerosol properties with IMPROVE, MODIS, and AERONET data. *J. Geophys. Res.* 112, D14301. doi:10.1029/2006JD008085.
- Saaroni, H., Ziv, B., Bitan, A., Alpert, P., 1998. Easterly wind storms over Israel. *Theor. Appl. Climatol.* 59, 61–77. doi:10.1007/s007040050013.
- Sanz, M.J., Calatayud, V., Calvo, E., 2000. Spatial pattern of ozone injury in Aleppo pine related to air pollution dynamics in a coastal-mountain region of eastern Spain. *Environ. Pollut.* 108, 239–247.
- Schaap, M., van Loon, M., ten Brink, H.M., Dentener, F.D., Builtjes, P.J.H., 2004. Secondary inorganic aerosol simulations for Europe with special attention to nitrate. *Atmos. Chem. Phys.* 4, 857–874.
- Schell, B., Ackermann, I.J., Hass, H., Binkowski, F.S., Ebel, A., 2001. Modeling the formation of secondary organic aerosol within a comprehensive air quality model system. *J. Geophys. Res.* 106 (D22), 28275–28293. doi:10.1029/2000JD003884.
- Shankar, U., Bhawe, P.V., Vukovich, J.M., Roselle, S.J., 2005. Initial application of sea salt emissions and chemistry algorithms in the CMAQv4.5-AERO4 module. In: In the 2005 Models-3 Users Workshop Chapel Hill, North Carolina, September 26–28.
- Sicard, M., Rocadenbosch, F., Reba, M.N.M., Comerón, A., Tomás, S., García-Vizcaino, D., Batet, O., Barrios, R., Kumar, D., Baldasano, J.M., 2011. Seasonal variability of aerosol optical properties observed by means of a Raman lidar at an EARLINET site over Northeastern Spain. *Atmos. Chem. Phys.* 11, 175–190.
- Skamarock, W.C., Klemp, J.B., 2008. A time-split nonhydrostatic atmospheric model for weather research and forecasting applications. *J. Comput. Phys.* 227 (7), 3465–3485. doi:10.1016/j.jcp.2007.01.037.
- Smyth, S.C., Jiang, W., Roth, H., Moran, M.D., Makar, P.A., Yang, f., Bouchert, W.S., Landry, H., 2009. A comparative performance evaluation of the AURAMS and CMAQ air quality modeling systems. *Atmos. Environ.* 43, 1059–1070.
- Spicer, C.W., Koetz, J.R., Keigley, G.W., Sverdrup, G.M., Ward, G.F., 1981. A Study of Nitrogen Oxides Reactions within Urban Plumes Transported over the Ocean. US-EPA, Research Triangle Park, NC.
- Talbot, R.W., Harrison, R.C., Browell, E.V., Gregory, G.L., Sebacher, D.I., Beck, S.M., 1986. Distribution and geochemistry of aerosols in the tropical north Atlantic troposphere: relationship to Saharan dust. *J. Geophys. Res.* 91 (D4), 5173–5182.
- Tarrasón, L., Iversen, T., 1998. Modelling intercontinental transport of atmospheric sulphur in the northern hemisphere. *Telus B.* 50 (4), 331–352.
- Tsyro, S., Simpson, D., Tarrasón, L., Klimont, Z., Kupiainen, K., Pio, C., Yttri, K.E., 2007. Modeling of elemental carbon over Europe. *J. Geophys. Res.* 112, D23S19.
- Viana, M., Querol, X., Alastuey, A., Cuevas, E., Rodríguez, S., 2002. Influence of African dust on the levels of atmospheric particulates in the Canary Islands air quality network. *Atmos. Environ.* 36, 5751–5875.
- Venkatram, A., Pleim, J., 1999. The electrical analogy does not apply to modeling dry deposition of particles. *Atmos. Environ.* 33, 3075–3076.
- WHO, 2006. WHO Europe Air Quality Guidelines for Particulate Matter, Ozone, Nitrogen Dioxide and Sulfur Dioxide. Global Update 2005. World Health Organization. Available at: http://www.euro.who.int/_data/assets/pdf_file/0005/78638/E90038.pdf.
- Yu, S., Dennis, R., Roselle, S., Nenes, A., Walker, J., Eder, B., Schere, K., Swall, J., Malm, W., Robarge, W., 2005. An assessment of the ability of three-dimensional air quality models with current thermodynamic equilibrium models to predict aerosol NO₃. *J. Geophys. Res.* 110, D07S13.
- Zakey, A.S., Giorgi, F., Bi, X., 2008. Modeling of sea salt in a regional climate model: fluxes and radiative forcing. *J. Geophys. Res.* 113, D14221. doi:10.1029/2007JD009209.
- Zhang, Y., Seigneur, C., Seinfeld, J.H., Jacobson, M., Clegg, S.L., Binkowski, F.S., 2000. A comparative review of inorganic aerosol thermodynamic equilibrium modules: differences, and their likely causes. *Atmos. Environ.* 34, 117–137.
- Zhang, K., Knipping, E., Wexler, A., Bhawe, P., Tonnesen, G., 2005. Size distribution of sea-salt emissions as a function of relative humidity. *Atmos. Environ.* 39, 3373–3379.